

This is the **accepted version** of the review article:

Sciortino, Giuseppe; Maréchal, Jean-Didier; Garribba, Eugenio. «Integrated experimental/computational approaches to characterize the systems formed by vanadium with proteins and enzymes». *Inorganic Chemistry Frontiers*, Vol. 8, Issue 8 (April 2021), p. 1951-1974. DOI 10.1039/d0qi01507e

This version is available at <https://ddd.uab.cat/record/288722>

under the terms of the  ^{IN} COPYRIGHT license

Integrated experimental/computational approaches to characterize the systems formed by vanadium with proteins and enzymes

Received 00th January 20xx,
Accepted 00th January 20xx

DOI: 10.1039/x0xx00000x

Giuseppe Sciortino,^{*a,b,c} Jean-Didier Maréchal,^a and Eugenio Garribba^{*b}

Decoding the interactions of transition metal complexes with proteins is still an open challenge in many fields like biology and medicinal chemistry or in the design of *de novo* enzymes, including artificial metalloenzymes. Instrumental techniques like X-ray crystallography or Nuclear Magnetic Resonance can provide with an atomistic description of the systems although their application is often not trivial. In this review we illustrate how the integrated approach based on spectrometric and spectroscopic techniques with multilevel Molecular Modelling allows characterizing metallodrug–protein adducts at molecular level. A series of applications are described, focusing on potential vanadium drugs with a final generalization to other metals. The data provide with major proof-of-concept on the power of coupled experimental and theoretical methods for the rational design of new metallodrugs as well as for guiding a large number of fields of bioinorganic chemistry.

1. Introduction

Understanding the biospeciation of potential metallodrugs in the organisms is one of the open challenge of this century in medicinal inorganic chemistry.^{1, 2, 3, 4} Metallocompounds (MCs) are generally prodrugs that undergo a wide range of *in vivo* chemical transformations along the “travel” to reach their targets inside cells.^{5, 6, 7} Biotransformations may include redox reactions at the metal center, ligand exchange and/or reactions of the organic functionalities of the ligands far from the metal. Clear understanding of these events at the molecular level appears to be fundamental to rationally design new prodrugs able to undergo conversion to the active species where and when their pharmacological effect is required. Endogenous bioligands, and particularly proteins, play a central role in the biotransformation processes, in particular those that are abundant in the bloodstream including human serum transferrin (HTf), human serum albumin (HSA), immunoglobulins (Ig) and hemoglobin (Hb).⁸ In a similar way, the interaction of metallic species with macromolecular hosts has a major application in biotechnology from the development of metallopeptides to the *de novo* design and redesign of enzymes.^{9, 10} In the latter cases, the catalytic activity and selectivity of the process can be handled introducing the proper interactions at the cofactor-biomolecule interface, *e.g.*

favouring those that stabilize the cofactor in a specific region or with a determined orientation for the reaction to take place.

In view of the rational design either of specific active MCs and accurate drug delivery strategies or catalytically active metal-based cofactors, deciphering the interaction of metal moieties with proteins is foundational. Primary information includes the number of binding sites able to host the MCs and their description at molecular level bringing insights on those interactions that stabilise or hinder the MC–protein adduct formation. The total electric charge of the MCs, the steric hindrance of the ligands, the nature of their substituents promoting stabilizations by secondary interactions – hydrogen bonds (*H-bonds*) and van der Waals (vdW) contacts – should be taken into account at the design stage. An accurate choice of the metal centres and their organic ligands enables to accurately balance the interactions strengths of MCs with the biological host depending on the desired binding affinity.

On one hand vanadium compounds (VCs) are receiving growing interest in medicine for their potential against parasite and viral infections such as HIV and tuberculosis and –especially – for their antidiabetic and antitumor activity.^{11, 12, 13, 14, 15, 16, 17, 18, 19, 20, 21} Since '80s of the last century, it was demonstrated that vanadate(V)²² and oxidovanadium(IV)²³ inorganic salts enhance the insulin effect in patients suffering from type II diabetes either inhibiting intracellular tyrosine phosphatase (PTP-1B) or activating cytosolic tyrosine kinase (cyt-PTK) and leading to the signal transduction cascade for glucose uptake. In addition to the inorganic species, bis-chelated V^{IV}O²⁺ coordination compounds (V^{IV}OL₂, being L a monoanionic bidentate organic ligand) have been successfully proposed for the antidiabetic treatment.^{24, 25, 26} However, the search for more efficient and

^a Departament de Química, Universitat Autònoma de Barcelona, Cerdanyola del Vallès, Barcelona E-08193, Spain.

^b Dipartimento di Chimica e Farmacia, Università di Sassari, Via Vienna 2, I-07100 Sassari, Italy. E-mail: garribba@uniss.it

^c Current address: Institute of Chemical Research of Catalonia (ICIQ), Avda. Països Catalans, 16, E-43007 Tarragona, Spain. E-mail: gsciortino@iciq.es.

side-effect free VCs is still an open mission.^{18, 24, 27} On the other hand, the artificial metalloenzymes (ArMs) community could exploit the high availability of V, its higher biocompatibility compared with other heavy metals, and catalytic properties toward asymmetric oxidation and C–C coupling reactions among others.^{28, 29, 30, 31} However, from the pioneering studies in the late '90 by Allenmark³² and Wever³³ on semi-synthetic haloperoxidases, and Sheldon^{34, 35, 36} on phytase, little was done in the field of V-based ArMs.^{37, 38} The reasons of the little progress in the above mentioned promising fields could be partially ascribed to the lack of structural and mechanistic knowledge of V-containing biosystems, which is one of the main factors for which VCs are not or little considered by the pharmaceutical companies.²⁷

In general, two types of binding are expected for a VC–protein system: i) *coordinative* (or *covalent*) binding for which the protein replaces L^- or another weak ligand, typically H_2O , with one or more donor-containing residues resulting in the formation of binary ($V^{IV}O_2^+$ –protein or $V^{VO}_2^+$ –protein) and ternary ($V^{IV}VOL$ –protein or $V^{IV}VOL_2$ –protein) adducts;³⁹ ii) *inert* (or *non-covalent*) binding in which the intact complex $V^{IV}OL_2/V^{VO}_2L/V^{VO}_2L_2$ binds only through secondary interactions with accessible groups of the protein surface.^{40, 41, 42}

Despite major progresses over the last years, the prediction and elucidation of the exact binding mechanism of metal moieties (being naked or complexed ions) is still a challenging question. In addition to X-ray diffraction (XRD), several spectroscopic techniques such as XANES, XAFS, NMR, EPR, ESEEM, ENDOR, UV-Vis and CD are routinely applied for the characterization of metal–protein adducts,^{43, 44} and have been widely employed for systems containing the most stable oxidation states of VCs, i.e. V^{III} , V^{IV} and V^V .⁴⁵ Among these techniques, X-ray and NMR, which in principle can provide with three dimensional information of any MC–protein adduct, are often inapplicable or give only a partial information on the binding region (e.g. for the lability of the metallodrug–protein interaction under crystal conditions and electron beaming, open shell systems, etc.). More recently, other methods such as voltammetry and polarography, HPLC-ICP-MS, size-exclusion chromatography, gel-electrophoresis, MALDI-TOF^{46, 47} and ESI-MS have joined the arsenal of bioinorganics. Among them, ESI-MS enables to study both *coordinative* and *inert* binding of metallodrugs, works independently of the oxidation state, clarifies the equilibria established in solution, and provides with the stoichiometry of the metal–protein adducts.^{48, 49} In the context of VCs, its working range of 1–100 μM , close to the medical and pharmacological concentrations,^{7, 24, 26} makes this technique a valuable ally.⁵⁰ On the other hand EPR, being the most powerful spectroscopic tool for paramagnetic species, has been largely applied for V^{IV} species, allowing to achieve relevant information on the nature of donor-containing residues involved in protein metalation and to discern between *coordinative* or *inert* binding.^{51, 52}

Nevertheless, in most of the cases the instrumental approach does not allow identifying neither the specific region of the protein where the metal binds and the residues involved in the interaction nor the stabilizations of the metallodrug by secondary intermolecular forces.

Computational methods can represent a valuable complementary approach to experiments providing with three dimensional models and reaction mechanisms.^{1, 41, 42, 53, 54, 55} However, a complete simulation of the metal binding should take into account various factors: i) an exploration of the protein conformations to detect the possible binding site(s) and ii) an analysis of the changes of first metal coordination sphere during the binding (for example, changes in the coordination and ligand number and/or geometry distortion).⁵⁶

In this review, we will discuss how to complement the information provided by spectroscopy and spectrometry with the computational methods. We will demonstrate that, in absence of a XRD analysis, only an integration of experimental techniques can bring to a complete characterization of complex systems such as metal–protein. We will focus on three main points. The first is the update of the docking methods for metallodrugs binding prediction and the specific validation for VCs and a presentation of the techniques – particularly, EPR and ESI-MS – that can be used to study several systems containing VCs and proteins. The method proposed here is actually capable of predicting with high accuracy both *coordinative* and *inert* binding. The second point, in which we will discuss a series of examples from our and other research groups, deals with the integration of spectrometric and spectroscopic partial information with a multilevel Molecular Modelling strategy, that allows to characterize VC–protein adducts at molecular level as well as their reaction mechanism in ArMs. Moreover, dynamics effects such as equilibria in the biological environment as well as conformational changes of the protein scaffold, achievable even in absence of X-ray or NMR data, will be treated. In the final section, a generalization to other metals will be presented.

2. Toward an efficient computational strategy

From a computational point of view, localizing the protein binding region and the modes of interaction of metallospecies entails a complex series of molecular variables.¹ The dynamic nature of both host and guest requires an advanced knowledge of the system under analysis. The metallocompounds may undergo ligand exchange or geometric reorganization prior the binding, as well as the protein can react with conformational changes leading to different adducts with respect to the original reactants. The interactions governing the binding can range from pure electrostatic, vdW or *H-bonds* for the ligands, to direct coordination bond for metals. On the *coordinative* binding framework, the most common protein donors are the amino acid side-chains whose affinity depends on the *hard* or *soft* character of the metal.⁵⁷

A unique computational technique able to tackle together all these variables is nowadays a chimera, thus different computational methods must be used in an integrated strategy to address the main steps during the metal–protein recognition process.^{1, 56, 58, 59, 60, 61, 62, 63, 64, 65, 66} Density Functional Theory (DFT), treating the chemical systems at electronic level, can describe with high accuracy the geometry, the equilibria, the spectroscopic properties as well as the reactivity of

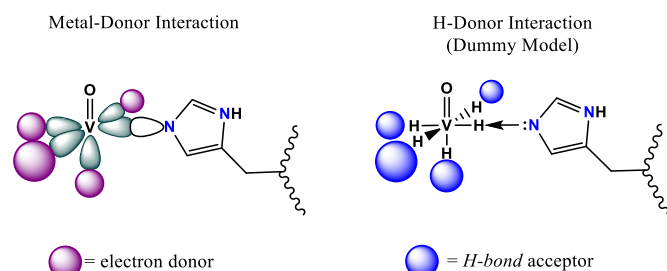


Fig. 1 Description of the dummy hydrogen approach for the metal ion docking to proteins. The optimal distance between the metal and the hydrogen that acts as a dummy was fixed at 0.75 Å. The *H-bond* mean distance, 2.9 Å in the original scoring function, was set to 1.9 Å.

coordination complexes giving information on their speciation in solution.^{53, 67, 68, 69, 70, 71, 72, 73} DFT, integrated with instrumental data (*vide infra*), is the first step of the simulation because it can individuate the chemical form of the MCs for binding. Molecular Mechanics (MM) based approaches, defining the system under the laws of the classical physics, are common on structural studies of protein systems including those containing metalloproteins. Among the MM based techniques, Molecular Dynamics (MD) is applied for studying conformational changes of high flexible regions of the receptor or of small peptides, and constitutes the first step of a subsequent metal binding analysis based on most sampled conformations (see section 3.1). Still within MM framework, protein–ligand docking methods were designed for fast and accurate prediction of the binding sites and modes of small molecules to proteins (in docking terminology *ligand* is the small molecule that interacts with protein[#]). The binding energy is computed through simplified MM force-fields (*Scoring Function*, SF) taking into account only non-bonded intermolecular interactions between the *ligand* and the protein host. The docking concept is to find, generally through a Genetic (GA) or a Montecarlo (MC) algorithm, a series of protein–ligand relative positions (*poses*), evaluate their binding energy and rank them by scoring.^{64, 74, 75, 76, 77, 78} Unfortunately, most of the available docking suites work with *ligands* constituted by organic species and dealing with coordination bond formation is ruled out, particularly when the metal is part or represents *per se* the *ligand* (metallo–ligands). Generally, the coordination bonds can be only described with pure electrostatic functions,^{79, 80, 81} or through *covalent docking* approaches nowadays implemented in many programs such as GOLD⁸² or Autodock,⁸⁰ or source code modifications such as CovalentDock⁸³ or Docketite.⁸⁴ For the formers, the specific protein–ligand bond needs to be defined *a priori* and forced during docking. Therefore, their applicability is limited to systems for which the specific bonded atom pairs are already known, fact that significantly limits the predictive capabilities of the method. Moreover, coordination bond parametrization is totally lacking in SF, ruling out the correct application of *covalent docking* to metallo–ligands. A few of other approaches have been proposed over the last years such as QM based SF.^{61, 85, 86}

2.1 Prediction of the *coordinative* binding

About a decade ago, we put the grounds for a generalizable approach for dealing with metals in protein–ligand dockings

that was tested on ArMs,^{87, 88} and *inert* metallodrugs.⁸⁹ We recently expanded and further validated this docking approach on the GOLD software framework defining the *coordinative* bond through the *H-bond* function included in *GoldScore* SF⁹⁰ without source code modifications. The metal is virtually described as a hydrogen bond donor liable to interact with the *H-bond* acceptors of protein by means of dummy atoms at the coordination vacancies. In terms of Lewis acid and base theory, the acid center is transferred along the bond axis from the metal to a fictitious proton located at the coordination vacancy (Fig. 1). In *GoldScore* SF (eq. 1⁹⁰), *H-bonds* are described by the S_{hbond}^{ext} term, a Lennard-Jones like function,⁹⁰ which is multiplied by a force constant defined for each atom pairs and able to describe bond lengths and angles, weighting its potential by a block function (eq. 2).

$$Fitness (F) = \alpha \cdot S_{hbond}^{ext} + \beta \cdot S_{vdW}^{ext} + \gamma \cdot S_{hbond}^{int} + \delta \cdot (S_{vdW}^{int} - S_{tors}) \quad \text{eq. 1}$$

where S_{hbond}^{ext} and S_{vdW}^{ext} describe the *H-bond* and vdW intermolecular interactions, S_{hbond}^{int} and S_{vdW}^{int} the intramolecular interactions, and S_{tors} evaluates the change in stability due to molecular torsions; α , β , γ , and δ are empirical parameters optimized to weigh the different interactions.

$$x_{wt}(x, x_{ideal}, x_{max}) = \begin{cases} 1, & \text{if } x < x_{ideal} \\ 1.0 - \frac{x - x_{ideal}}{x_{max} - x_{ideal}}, & \text{if } x_{ideal} \leq x \leq x_{max} \\ 0, & \text{if } x > x_{max} \end{cases} \quad \text{eq. 2}$$

The hard work consisted in generating the convenient atom types and coordination forces to adapt this idea to GOLD without using any geometrical constraint or energy restraint. The strength of the *coordinative*-like interactions between 15 metals (Mg, V, Cr, Mn, Fe, Co, Ni, Cu, Zn, Ru, Rh, Re, Os, Pt, Au) and all the amino acid acceptors are defined by a series of empirical parameters, implemented in *GoldScore*, to take into account their relative affinity toward each metal.^{41, 55} The model has been first validated on a set of 39 high-quality X-ray structures with a unique *coordinative* M–donor bond.⁵⁵ A second step along the way was to generalize the framework for the binding of metallo–ligands with more than one vacant site. The benchmark was augmented to 64 structures formed by main group- and transition metal-containing *ligands* with various coordination numbers (4–6), geometries (square planar, tetrahedral, trigonal bipyramidal, square pyramidal, and octahedral), and accessible coordination sites.⁴¹ The results showed an excellent agreement between the predicted and crystallographic structures, indicating that the method could be used as a new tool to predict metallocomplex–protein interactions.

Further efforts in the context of (metal ion)–protein binding are represented by the coordination gene implemented in GaudiMM,^{91, 92} and the recent backbone preorganization hypothesis developed within the software BioMetAll.⁹³

2.2 Prediction of the *inert* binding

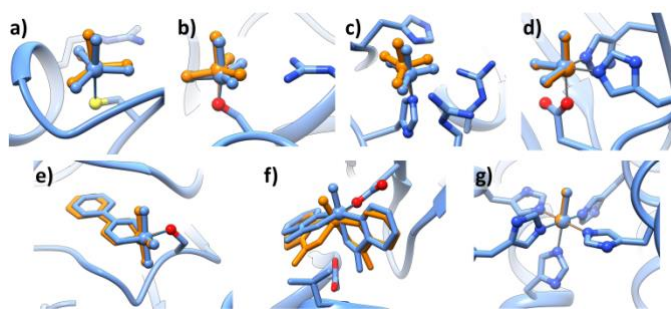


Fig. 2 Superimposition of the calculated (in yellow) and X-ray (in green) structures for V^V -protein and V^{IV} -protein adducts: a) V^VO_4 moiety bound to tyrosin phosphatase (PDB: 3i80); b) V^VO_4 bound to alkaline phosphatase (PDB: 1b18); c) V^VO_4 bound to acid phosphatase (PDB: 1rpt); d) $V^{IVO}O^{2+}$ bound TauD (PDB: 1edh); e) V^VO_3 (benzohydroxamate) bound to chymotrypsin A (PDB: 2p8o); f) V^VO (picolinato)₂ bound to lysozyme (PDB: 4c3w); and g) $V^{IVO}O^{2+}$ moiety bound CH_3Y^* variant of cyt *cb*₅₆₂ (PDB: 1dyl).

On the framework of *inert* or *non-coordinative* binding, several docking software offers the opportunity to treat metallo-ligands.^{79, 80, 81, 88, 89}

Using *GoldScore* SF, the coefficients α , γ , and δ to weigh the intermolecular and intramolecular *H-bonds* and vdW interactions are 1.0, while β for intermolecular vdW contacts is 1.375. For metal complexes, this combination could overestimate vdW compared to *H-bonds*. Therefore, to reproduce the experimental results – depending mainly on the features of the organic ligands coordinated to the metal – it could be necessary to tune the values of the terms α and β to balance the relative weight of the *H-bond* and vdW contacts. In other words, if the structure of the ligands is such that several hydrogen bonds with polar groups exposed on the protein surface can be formed, the weight of α must be higher than β and modulated as a function of the ligand functionalities able to interact with the protein.

In this context, in 2018 a modification of the *GoldScore* SF was set to accurately reproduce *non-covalent* binding affinity of potential drugs with formula $V^{IV}OL_2$ to proteins (see *infra*).⁴²

2.3 Validation for VCs

In the context of VCs, the methodology to predict the *coordinative* bonds has been extensively validated on the available X-ray structures in the protein data bank (PDB), namely V^VO_3 (benzohydroxamate) bound to chymotrypsin A with the coordination of a Ser-O⁻ (PDB: 2p8o⁹⁴); V^VO_4 moiety bound to acid, alkaline, and tyrosine phosphatase with the binding of a His-N, Ser-O⁻, and Cys-S⁻ donors (PDB: 1rpt⁹⁵, 1b8j⁹⁶, and 3i80⁹⁷, respectively); *cis*- V^{IVO} (picolinato)₂ moiety to lysozyme (Lyz) through the equatorial coordination of Asp-COO⁻ donor (PDB: 4c3w⁹⁸); the $V^{IVO}O^{2+}$ adducts with α -ketoglutarate-dependent taurine dioxygenase (TauD, PDB: 6edh⁹⁹) and cyt *cb*₅₆₂ variant (CH_3Y^* , PDB: 6dyl¹⁰⁰).

The predictiveness of the method was ensured considering: i) full rotation of the metallo-ligand dihedral angles; ii) the flexibility of the coordinating side-chains using the rotamer libraries available in the literature;¹⁰¹ iii) the unbiased metal free structure of protein, when available, to ascertain the applicability of the technique even starting from an apo structure.

The *GoldScore* scoring function improved with new set of optimized parameters leads to docking solutions with reasonably binding affinities (F_{max} in the range 28.4–62.4). In all of the cases, the predicted bindings matched with the experimental ones obtaining root mean square deviation (RMSD) with respect to the X-ray structures ranging from 0.039 Å for the ions up to 1.035 Å for the coordination compounds, values confirming a satisfactory prediction (Fig. 2).^{102, 103, 104} The “*coordinative*” energetic terms implemented in *GoldScore* are reported in refs.^{41, 54, 55}

3. Integrating experiments and simulation

To characterize completely a VCs–protein systems is necessary to choose instrumental techniques that provide complementary information which can represent the starting point to carry out the computational protocol. As mentioned above, electron paramagnetic resonances (EPR) and electrospray ionization mass spectrometry (ESI-MS) will be taken to illustrate the approach. It must be highlight here that ESI-MS is applicable to any metal, while EPR is the best tool for paramagnetic V^{IV} and should be replaced by other techniques with other metal centres (for example, NMR for V^V or UV-Vis for V^{III}).

3.1 EPR spectroscopy

Electron Paramagnetic Resonance (EPR) is a spectroscopic technique applicable, in principle, to any paramagnetic compound with one or more unpaired electrons. When a mononuclear paramagnetic species with only one unpaired electron is considered, the spectrum is characterized by two spin Hamiltonian parameters: the *g* factor and the hyperfine coupling (HFC) constant between the unpaired electron and metal nucleus (g_{iso} and A_{iso} in an *isotropic* spectrum, and g_x , g_y , g_z and A_x , A_y , A_z in a *rigid limit* or *anisotropic* spectrum).¹⁰⁵ The *g* and *A* tensors are strongly perturbed by the metal chemical environment and their change could provide valuable information on the structure of the metal species under examination. In particular, the values of g_z and A_z are more sensitive to the coordination sphere variations than the *x* and *y* components.

For V^{IV} , d^1 configuration and one unpaired electron, the HFC constants in the EPR spectra arise from the interaction between the spin-angular momentum of the electron ($S = 1/2$) with the spin-angular momentum of the ⁵¹V nucleus ($I = 7=2$, 99.8% natural abundance). With increasing the electron donor capability of the ligands, an increase of the experimental value of g_z and a decrease of A_z is observed.

For small complexes a *rigid limit* spectrum is expected in frozen solutions (for example, at liquid nitrogen temperature) because the molecules are blocked in their positions, and *isotropic* spectrum at room temperature due to the rotational motion faster than the EPR timescale (usually around 50 ns¹⁰⁶). In contrast, for large $[V^{IV}OL_x]$ -Protein adducts, a *slow tumbling* or a *rigid limit* spectrum is ever expected because their rotational motion is significantly slowed down:¹⁰⁷ the slower the rotational

motion, the more the spectrum approaches the *rigid limit* type.¹⁰⁸

Nowadays, the spin Hamiltonian parameters, in particular HFC ^{51}V \mathbf{A} tensor, can be predicted by DFT methods.^{70, 109, 110, 111, 112} In most of the cases, this allows to confirm the binding coordination environment of a V–protein comparing the experimental with calculated A_z .⁵³ For a $\text{V}^{\text{IV}}\text{O}$ adducts the combination of the functional BHandHLYP and the basis set 6-311g+(d) gives the best results with a percent deviation of A_z^{calcd} from A_z^{exptl} below 3%.⁷³

3.2 ESI-MS technique

Instrumental techniques based on mass spectrometry (MS) such as Electrospray Ionization Mass Spectrometry (ESI-MS) and Matrix Assisted Laser Desorption Ionization Mass Spectrometry (MALDI-MS) are the most powerful techniques to analyse the precise interactions of metallodrugs with biomolecules, including DNA and proteins. ESI-MS generates ions with a single or multiple charges after the formation of adduct with protons, alkali metal ions (especially, Na^+ or K^+) or after deprotonation, resulting in a characteristic charge envelope for peptides, proteins and oligonucleotides.^{113, 114, 115}

Up to now, the major applications concerned the exploration of inert metal complexes formed by Ru, Pt, and Au to low molecular mass bioligands such as DNA nucleic bases, amino acids, oligonucleotides and peptides, and high molecular mass biomolecules such as proteins.^{116, 117, 118, 119} However, being a soft technique, it has been suggested that ESI-MS can also be applied to the study of metal complexes that form labile coordinative bonds, such as copper and vanadium,^{49, 50, 120} and of *non-covalent* interactions with the biomolecules of organism.^{48, 49} It has recently been used to study the interaction of pharmacologically active VCs with model proteins and amavadin.⁵⁰

ESI-MS presents several aspects that make it an almost ideal technique for studying metal–protein systems. It allows to: i) identify both *covalent* and *non-covalent* interactions; ii) suggest if a metal complex exists in the free form or bound to a protein; iii) determine the type and the number of metal moieties ($n[\text{ML}]$, $n[\text{ML}_2]$, $n[\text{ML}_3]$ and others, where $n = 1, 2, 3$, etc.) interacting with proteins; iv) reveal, for vanadium, the contemporaneous presence in aqueous solution of adducts formed by various metal oxidation states (V^{III} , $\text{V}^{\text{IV}}\text{O}/\text{V}^{\text{IV}}$ and $\text{V}^{\text{VO}}/\text{V}^{\text{VO}_2}$); v) examine metal concentrations in the range 1–100 μM , therefore very close to those found for vanadium at the physiological conditions⁷.

The main limitation is that it often does not provide information: i) on the three-dimensional structure of the revealed adducts; ii) on the identity of the side-chain amino acid donors, and iii) on the relative amount of species in solution since the intensity of the peaks cannot be directly related with their concentration.

3.3. Integrated strategy for coordinative binding

When X-ray or NMR determinations of MCs–protein adducts are not possible, other instrumental approaches like

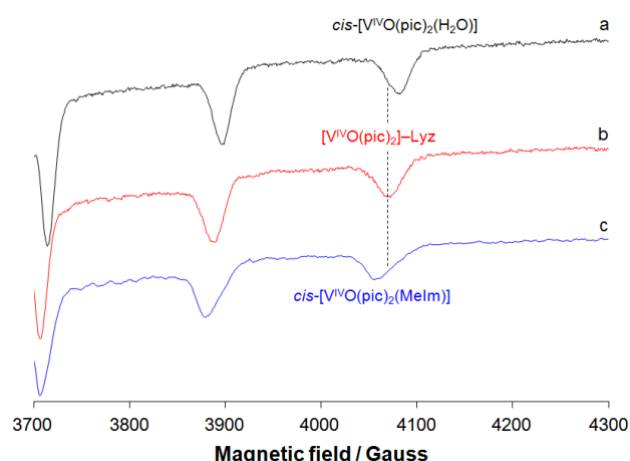


Fig. 3 High-field region of anisotropic X-band EPR spectra recorded at 120 K in aqueous solution containing: a) $\text{V}^{\text{IV}}\text{O}^{2+}/\text{pic}$ 1/2 at pH 4.5 ($\text{V}^{\text{IV}}\text{O}^{2+}$ 1.0×10^{-3} M); b) $\text{V}^{\text{IV}}\text{O}^{2+}/\text{pic}/\text{Lyz}$ 1/2/8 at pH 4.5 ($\text{V}^{\text{IV}}\text{O}^{2+}$ 4.4×10^{-4} M); and c) $\text{V}^{\text{IV}}\text{O}^{2+}/\text{pic}/\text{Melm}$ 1/2/4 at pH 7.4 ($\text{V}^{\text{IV}}\text{O}^{2+}$ 1.0×10^{-3} M). The $M_I = 7/2$ resonance of the adduct $[\text{V}^{\text{IV}}\text{O}(\text{pic})_2]\text{-Lyz}$ was indicated with the dotted line. Pic denotes picolinato ligand and Melm 1-methylimidazole. Adapted from ref. 54.

spectroscopy and spectrometry could provide with partial information. These pieces could be joined by molecular modelling obtaining a complete structural characterization of the system.

Having at hand the X-ray resolution of the $[\text{VO}(\text{pic})_2]\text{-Lyz}$ adduct (where pic is the picolinato monoanionic ligand[†]),⁹⁸ we set up a validation test with the aim to reproduce the experimental structure basing only on spectroscopic data and theoretical simulations: i) EPR data of the binary system $\text{V}^{\text{IV}}\text{O}^{2+}/\text{pic}$ in solution were coupled with DFT simulation obtaining, among all the possible isomers, those of higher stability; ii) EPR of the ternary system $\text{V}^{\text{IV}}\text{O}^{2+}/\text{pic}/\text{Lyz}$ were collected evaluating the specific donors involved in the metal coordination; iii) blind docking calculations were performed between the DFT optimized structures of $\text{V}^{\text{IV}}\text{O}(\text{pic})_2$ moiety and the X-ray structure of Lyz; iv) the values of ΔG_{bind} for the formation of the adduct $[\text{V}^{\text{IV}}\text{O}(\text{pic})_2]\text{-Lyz}$ were calculated by QM/MM; v) NCI (Non-Covalent Interactions¹²¹) plot surface were built to determine the stabilization of the adduct by non-covalent contacts.⁵⁴

The analysis of the binary system unveils a clear preference for the *cis*-octahedral isomers^{122, 123} and, among the four possible geometrical isomers of *cis*- $[\text{VO}(\text{pic})_2(\text{H}_2\text{O})]$ ¹²⁴, those with two equatorial nitrogens (*OC*-6-23,24 with their respective Λ and Δ enantiomers) are strongly favoured and in equilibrium to each other.^{122, 123} The EPR spectrum recorded in the ternary system $\text{V}^{\text{IV}}\text{O}^{2+}/\text{pic}/\text{Lyz}$ (trace b of Fig. 3), compared with those of *cis*- $[\text{V}^{\text{IV}}\text{O}(\text{pic})_2(\text{H}_2\text{O})]$ (trace a of Fig. 3), and with $[\text{V}^{\text{IV}}\text{O}(\text{pic})_2(\text{Melm})]$ where Melm = 1-methylimidazole is a good model for His-N binding (trace c of Fig. 3), clearly indicates that Lyz binds $\text{V}^{\text{IV}}\text{O}^{2+}$ with a $\gamma/\delta\text{-COO}^-$ group, stemming from an Asp or Glu residue. The variation of A_z for $[\text{V}^{\text{IV}}\text{O}(\text{pic})_2]\text{-Lyz}$ ($163.3 \times 10^{-4} \text{ cm}^{-1}$) with respect to *cis*- $[\text{V}^{\text{IV}}\text{O}(\text{pic})_2(\text{H}_2\text{O})]$ ($165.0 \times 10^{-4} \text{ cm}^{-1}$ ¹²³) and to the model complex *cis*- $[\text{V}^{\text{IV}}\text{O}(\text{pic})_2(\text{Melm})]$ ($158.8 \times 10^{-4} \text{ cm}^{-1}$ ¹²⁵) indicates that Lyz coordinates $\text{V}^{\text{IV}}\text{O}$ through a donor stronger than water-O but weaker than His-N (see the position of the $M_I = 7/2$ resonances in Fig. 3). Taking these data into account, all the most stable isomers of *cis*- $[\text{V}^{\text{IV}}\text{O}(\text{pic})_2(\text{H}_2\text{O})]$ (*OC*-6-24- Λ/Δ ,

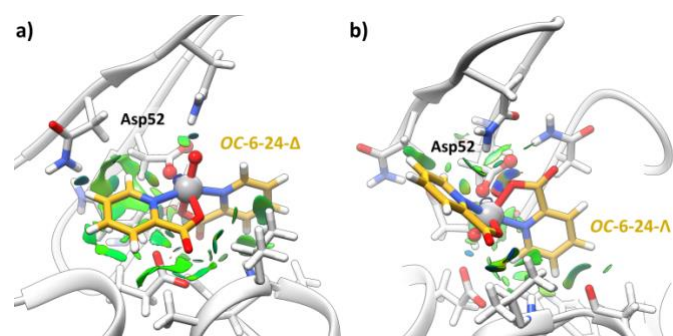


Fig. 4 Gradient isosurfaces ($s = 0.3$ a.u.) analysis of the better solution for the binding of $V^{IV}O(pic)_2$ moiety to lysozyme: a) isomer OC-6-23- Δ ; and b) isomer OC-6-24- Δ . NCIPLOT surfaces show only the intermolecular interactions. The surfaces are reported in a blue-green-red scale according to values of $sign(\lambda_2) \times \rho$, with ρ electron density and λ_2 the second Hessian eigenvalue. Blue surfaces indicate strong attractive interactions (such as dipole-dipole or hydrogen bond), red indicates repulsion, while green means van der Waals contacts. For further details on NCIPLOT the readers can refer to ref. 124.

OC-6-23- Δ) were DFT optimized and the equatorial H_2O removed activating the vacancy for *coordinative* docking. The energy minima of *cis*- $V^{IV}O(pic)_2$ moiety were blind docked to lysozyme obtaining that, among the eight possible isomers, OC-6-23- Δ presents the higher population and best affinity toward Lyz with coordination through the COO^- group of Asp52. Therefore, our docking strategy is able to reproduce the isomeric and chiral discrimination of the protein proposing as the best solution that matching with the experimental structure,⁹⁸ despite the four isomers OC-6-24- Δ , OC-6-23- Δ / Δ have comparable stability in solution as demonstrated by DFT calculations.^{122, 123}

To further validate the discriminative capabilities of the technique, the QM/MM ΔG for the reaction $[V^{IV}O(pic)_2(H_2O)] + Lyz \rightleftharpoons [V^{IV}O(pic)_2]_{-}Lyz + H_2O$ was computed for all the best solutions of the assay with the same trend obtained with the pure scoring interaction energies. The ΔG_{bind} of the adduct [OC-6-23- Δ - $V^{IV}O(pic)_2$]-Lyz(Asp52) resulted lower more than 6 kcal mol^{-1} than the second best solution. Finally, NCI examination allows finding the molecular features behind the chiral discrimination, highlighting that only OC-6-23- Δ isomer can coordinate Asp52 establishing stable second coordination sphere interactions (Fig. 4).

3.4 Integrated strategy for inert binding

In the context of *inert* binding, in 2018 we validated a modification of the *GoldScore* SF to accurately reproduce the binding affinity of $V^{IV}O$ compounds with proteins. For this purpose, a series of five bis-chelated $V^{IV}O$ flavonoid complexes with proven antitumor activity^{14, 141, 148-152} ($[VO(que)_2]^{2-}$, $[VO(mor)_2]$, $[VO(7,8-dhf)_2]^{2-}$, $[VO(chr)_2]$ and $[VO(5-hf)_2]$, while $[VO(acac)_2]$, $[VO(cat)_2]^{2-}$ were examined for comparison[†]) were used as a benchmark for the binding with Lyz.[‡]

As a first step, the EPR results were coupled with DFT simulations for determining the stable isomers of the complexes under examination: the geometry is square pyramidal and the free apical site is not prone toward coordination.¹²⁶ Some of the $V^{IV}O$ complexes give, at room temperature, an anisotropic EPR spectrum even if the protein does not interact through a *coordinative binding* (cf. traces a and b of Fig. 5). This means that the *inert* binding is strong enough to block the VCs on the protein surface, hindering their

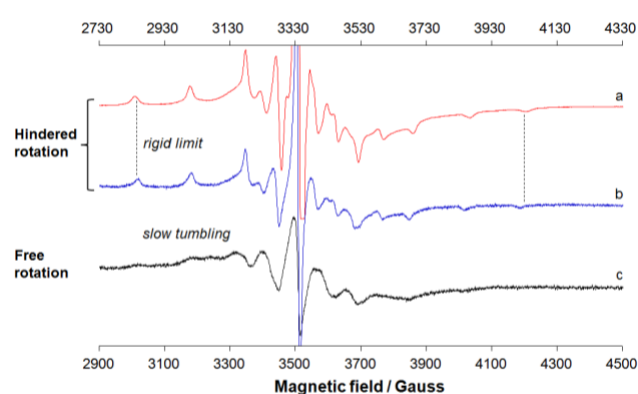


Fig. 5 X-band EPR spectra recorded at pH 7.40 on: a) binary system $V^{IV}O^{2+}/que$ 1/2 at 77 K and $\nu = 9.406$ GHz ($V^{IV}O^{2+}$ concentration 1.0×10^{-3} M); b) ternary system $V^{IV}O^{2+}/que/Lyz$ 1/2/1 at 298 K and $\nu = 9.852$ GHz ($V^{IV}O^{2+}$ concentration 7.0×10^{-4} M) and c) binary system $V^{IV}O^{2+}/que$ 1/2 at 298 K and $\nu = 9.852$ GHz ($V^{IV}O^{2+}$ concentration 7.0×10^{-4} M). The magnetic field in the upper axis refers to the trace a, and that in the lower axis to the traces b and c. With the dotted line the position of the $MI = -7/2, 7/2$ resonances of $[V^{IV}O(que)_2]^{2-}$ at 77 K are indicated. Adapted from ref. 42.

rotational motion and giving a *rigid limit* spectrum (see section 2.2).⁴² To explain this finding, it is necessary to postulate strong *H-bonds* due to the large number of $-OH$ groups in the flavonoid structure, able to block the motion of $V^{IV}O$ complexes in aqueous solution. Docking simulations were carried out fine tuning the weight of S_{hbond}^{ext} and S_{vdw}^{ext} terms of *GoldScore*, assigning the value 1.0 to α and 0.3 to β (see eq. 1), i.e. considering the weight of the intermolecular *H-bonds* ca. three times that of the vdW interactions. On the basis of the EPR data, an indicator to define the binding affinity has been extracted. The indicator is represented by the highest and average scoring (F_{max} and F_{mean}) obtained on a docking assay along 100 GA runs. A value of F_{max} in the range 16-17 marks the transition from the *rigid limit* to *slow tumbling* EPR spectrum (Table 1). The docking energetic breakdown highlights that the main contribution to the binding affinity is the number of free OH or CO groups in the structure of the organic ligand able to form *H-bonds* with the polar functionalities of the protein surface. Moreover, the results – showing that several binding sites for the same complex exist – could suggest a dynamical equilibrium with the VCs distributed among such sites (giving a *rigid limit* EPR spectrum) and free in solution (giving a *slow tumbling* spectrum).

Table 1 Docking results and EPR spectrum for *non-covalent* binding of VCs formed by flavonoid ligands with Lyz.^{a,b}

$V^{IV}O$ complex	EPR spectrum	OH / CO	F_{max}^c	F_{mean}^c
$[VO(mor)_2]$	<i>rigid limit</i>	4 / 0	22.7	18.6-21.3
$[VO(que)_2]^{2-}$	<i>rigid limit</i>	3 / 1	21.9	18.1-21.3
$[VO(7,8-dhf)_2]^{2-}$	<i>rigid limit with slow-tumbling resonances</i>	0 / 1	17.2	14.7-16.5
$[VO(chr)_2]$	<i>Slow-tumbling</i>	1 / 0	15.9	14.2-14.8
$[VO(5-hf)_2]$	<i>Slow-tumbling</i>	0 / 0	16.0	13.6-14.6
$[VO(acac)_2]$	<i>Isotropic</i>	0 / 0	12.5	12.5
$[VO(cat)_2]^{2-}$	<i>Isotropic</i>	0 / 0	10.4	10.0-10.4

^a Data were taken from ref. 42 and refer to the SPY-5-13 isomers that show the highest affinity. ^b The coefficient β has been changed and set to 0.3 (default value = 1.375) in the *GoldScore* SF, while the other parameters (α , γ and δ) were set to 1.0 (see eq. 1). ^c The value of 16-17 units marks the transition from a *rigid limit* to a *slow-tumbling* spectrum.

Overall, the proposed integrated EPR-computational approach enables to define if VCs strongly interact with a protein giving information about the stabilizing interactions as well as the delivery potential to a given target. Moreover, a careful combination of the docking data with ESI-MS could define the number and the nature of the sites available for binding (see section 4.2).

These insights should be taken into account during the design of novel drugs in order to balance such interactions as a function of the required affinity in view of a clear delivery strategy. It is important to note that the method is generalizable to any metallo-ligands tuning the contribution of the *H-bond* and vdW terms in the SF depending on the metal and on the structure of the organic ligand.

4. Applications

4.1 $V^{IV}O^{2+}$ binding

After oral or intravenous administration, VCs with potential application in medicine in their most stable +IV and +V oxidation states enter the bloodstream interacting with low and high molecular mass bioligands. *In vivo* blood circulation monitoring-EPR studies on rats demonstrated that at least 90% of vanadium is present in the +IV oxidation state,¹²⁷ but an equilibrium between V^{IV} and V^V under physiological conditions is plausible.^{5, 128} Among the possible interactions, those with serum proteins and erythrocytes must be mentioned due to their high concentration and affinity toward vanadium.⁷ Hemoglobin (Hb), human serum transferrin (hTf), immunoglobulin G (IgG) and human serum albumin (HSA) have been proposed as the main carriers of VCs in the bloodstream.^{6, 7, 8} The hydrolysis of VCs at medical concentrations causes the release of $V^{IV}O^{2+}$ from $V^{IV}OL_2$ potential drugs,⁷ leading to the insight that this species could be one of active forms in the organism and be responsible together with $[H_2V^{VO}_4]^-/[HV^{VO}_4]^{2-}$ of the V pharmacological effects.^{45, 129} Over the last years, we rationalized new and already collected instrumental data with a multi-level MM and full DFT based strategy to unveil the binding sites and modes of $V^{IV}O^{2+}$ ion with the serum proteins. Concerning HSA, which is one of the main transport protein of metal species in the blood, it displays several binding sites for different metals, namely the *N*-terminal site (NTS or ATCUN motif) specific for Cu^{2+} and Ni^{2+} , the multi-metal binding site (MBS or site A) with higher affinity toward Zn^{2+} and Cd^{2+} , and several sites B, preferential for Mn^{2+} and Co^{2+} , unknown until a few months ago.¹³⁰

To unveil the binding of $V^{IV}O^{2+}$ with both defatted (HSA^d) and fatted (HSA^f) albumins we applied an integrated strategy based on EPR spectroscopy, MD, docking and DFT methods.¹³¹ EPR spectra recorded on the binary system $V^{IV}O^{2+}/HSA^d$ as a function of pH and molar ratio display the signals of: i) a *primary* and a *secondary* site with similar A_z values compatible with two equatorial His-N plus a number of O donors stemming from carboxylates (Asp and/or Glu), carbonyl or H_2O and ii) *tertiary* weaker sites involving the coordination of only one His-N and O donors (Fig. 6). EPR competition studies with Zn^{2+} and Ni^{2+} ions

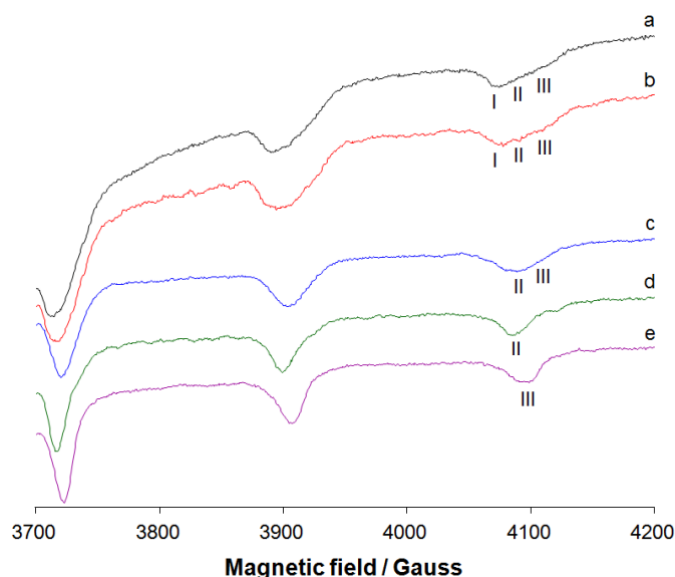


Fig. 6 High field region of the X-band anisotropic EPR spectra recorded at pH 7.4 on frozen solutions (120 K) containing: a) $V^{IV}O^{2+}/HSA^d$ 1/1; b) $V^{IV}O^{2+}/Zn^{2+}/HSA^d$ 1/1/1; c) $V^{IV}O^{2+}/Ni^{2+}/HSA^d$ 1/1/1; d) $V^{IV}O^{2+}/PSA$ 1/1 and e) $V^{IV}O^{2+}/Zn^{2+}/PSA$ 1/1/1. With I, II and III the $M_l = 7/2$ resonances of the sites NTS, MBS and 'tertiary' (sites B) are indicated. $V^{IV}O^{2+}$ concentration was 7.5×10^{-4} M in all cases. Adapted from ref. 131.

suggested that the *primary* site is located at the NTS, while the *secondary* one at the MBS; in fact, one equivalent of Ni^{2+} , that binds specifically at the NTS motif, shifts the EPR signal from I (NTS) to II (MBS, cfr. trace c with a and b of Fig. 6), while the addition of Zn^{2+} , which has its specific site at the MBS, leaves the spectra unaltered suggesting a slight competition with $V^{IV}O^{2+}$ that remains bound to its *primary* site (see resonance I and II in trace b of Fig. 6). These insights were confirmed using porcine serum albumin (PSA): in fact, with PSA $V^{IV}O^{2+}$ binds at MBS because His3 is lacking (II in the trace d of Fig. 6), but when Zn^{2+} is added it displaces from MBS $V^{IV}O^{2+}$ ion which moves to the tertiary sites (III in the trace e of Fig. 6).

In the light of these results, it was possible to characterize the binding sites at molecular level: i) a preliminary MD of HSA was carried out to collect a series of sampled conformations, particularly for the high flexible *N*-terminus; ii) using the software BioMetAll,⁹³ each conformation was probed for regions containing the motif (His; His; Asp/Glu) with the correct degree of preorganization to bind $V^{IV}O^{2+}$; iii) for each selected snapshot, docking simulations were performed obtaining first 3D structures; iv) these structures were then relaxed by further MDs and optimized by full DFT cluster method proposed by Siegbahn and Himo¹³²; v) in the last step, the ΔG_{bind} and spin Hamiltonian parameters at the level of theory BHandHLYP/6-311+g(d) were computed and compared to the experimental results allowing to obtain the final 3D structure of the *primary* and *secondary* adducts.

Overall, these data suggested that for NTS site the most stable binding mode is (His3-N, His9-N, Asp13-COO, Asp255-COO). For MBS, both modes MBS₁ (His67, His247, Asp249, H_2O) and MBS₂ (His67, His247, Asp249, Asn99) can be considered alternative with the difference represented by the fourth donor, one water-O or Asn-CO (Fig. 7, a and b).

Table 2 Donors, ^{51}V A_z and $\Delta E_{\text{binding}}$ for the 'primary' (NTS) 'secondary' (MBS) and dimeric binding sites of HSA for $\text{V}^{\text{IV}}\text{O}^{2+}$.

Site	Donors	A_z^{calcd} ^b	$\Delta E_{\text{binding}}$ ^c
NTS ₁ ^d	His3; His9; Asp13; Asp255	-163.7 ^e	-31.7
NTS ₂ ^d	His3; His9; Glu6; H ₂ O	-165.8 ^e	-18.4
MBS ₁ ^d	His67; His247; Asp249; H ₂ O	-165.2 ^f	-26.2
MBS ₂ ^d	His67; His247; Asp249; Asn99-CO	-169.5 ^f	-32.9
Dimer	Magnetic Coupling	J ^g	$\text{V}^{\text{IV}}\dots\text{V}^{\text{IV}}$ ^h
1	Ferromagnetic	19.9	3.164
2	Ferromagnetic	7.0	3.173

^a Data taken from ref. ¹³¹. ^b A_z calculated with DFT methods. ^c $\Delta E_{\text{binding}}$ in kcal mol⁻¹. ^d For HSA^d. ^e Experimental value for the NTS site is -162.9×10^{-4} cm⁻¹. ^f Experimental value for the MBS site is -166.4×10^{-4} cm⁻¹. ^g J value in cm⁻¹, determined with the method reported in refs. ^{133, 134}. ^h Distance between V atoms in Å.

The description of the $\text{V}^{\text{IV}}\text{O}^{2+}$ binding to HSA^d has been completed with an extensive analysis of the protein, searching for motifs (His-N, *n*Asp/Glu-COO) compatible with the EPR signals of the *tertiary* sites (III in Fig. 6). The sites with coordination (His367-N, Glu313-CO), (His510-N, Asp512-COO), (His338-N, Asp340-COO), (His535-N, Glu531-COO, Asn503-CO), (His288-N, Glu153-COO), and (His128-N, Glu131-COO) were found.

Finally, the binding of $\text{V}^{\text{IV}}\text{O}^{2+}$ to HSA^f has been characterized with an equivalent strategy. It must be highlighted that level of medium- and long-chain fatty acids (FAs) influence the binding of Zn^{2+} ,^{130, 135} inducing the rotation of subdomain IA with respect to the subdomain IIA,^{136, 137} and the disruption of the MBS separating the coordinating amino acids.^{138, 139, 140} The EPR analysis of the binary system $\text{V}^{\text{IV}}\text{O}^{2+}/\text{HSA}^f$ displays a complete different behaviour suggesting the formation of a dinuclear species with spin state $S = 1$, $(\text{V}^{\text{IV}}\text{O})_2(\text{HSA}^f)$.^{141, 142} A sequential docking assay has been carried out at the interface of subdomains IA and IIA of the XRD structure of HSA^f: i) a first $\text{V}^{\text{IV}}\text{O}^{2+}(\text{H}_2\text{O})_n^{2+}$ moiety was docked, followed by ii) subsequent docking of an additional $\text{V}^{\text{IV}}\text{O}^{2+}(\text{H}_2\text{O})_n^{2+}$ to the best solutions obtained in the first run. The resulting four dinuclear candidates were refined by full DFT cluster method and the exchange coupling constant J simulated. Only two candidates (1-2) showed a ferromagnetic coupling with a $\text{V}^{\text{IV}}\dots\text{V}^{\text{IV}}$ distance in agreement with EPR data (see Table 2 and Fig. 7).

The described integrated strategy have been used in a series of works to fully rationalize and characterize the binding sites of $\text{V}^{\text{IV}}\text{O}^{2+}$ to the other abundant serum proteins, namely Hb, apo-hTf¹⁴³ and holo-hTf, IgG as well as to model proteins such as ubiquitin (Ub)¹⁴⁴ and myoglobin (Mb).¹⁴⁵ We believe that, being $\text{V}^{\text{IV}}\text{O}^{2+}$ the most important active species released by antidiabetic and antitumor VCs, the characterization at molecular level of its binding sites could open new possibilities to understand the mechanism of action of novel V based drugs. We highlight in this case too that this approach is applicable to other free metal ions, coupling computational methods to the appropriate spectroscopic or instrumental techniques.

4.2 $\text{V}^{\text{IV}}\text{OL}_2$ potential drugs

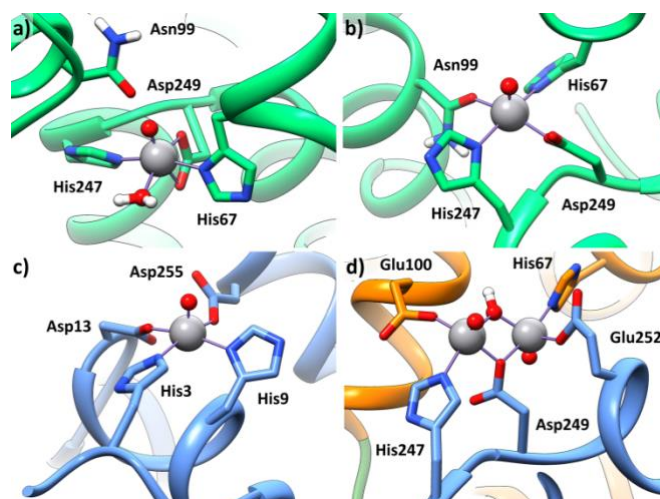


Fig. 7 Full DFT binding modes for $\text{V}^{\text{IV}}\text{O}^{2+}$ ion to HSA: a) mode MBS₁ of HSA^d; b) mode MBS₂ of HSA^d; c) NTS₁ mode of HSA^f; d) dinuclear species **1** ($\text{V}^{\text{IV}}\text{O})_2(\text{HSA}^f)$ at subdomain IA/IIA interface of HSA^f. Subdomains IA and IIA are shown in blue and orange, respectively. Adapted from ref. ¹³¹

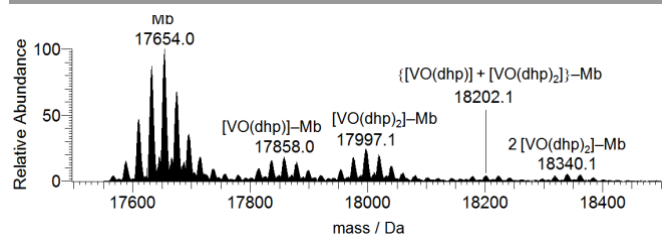


Fig. 8 Deconvoluted ESI-MS spectrum recorded on the system containing $[\text{V}^{\text{IV}}\text{O}(\text{dhp})_2]$ and myoglobin (5 μM) with molar ratio 5/1. Adapted from ref. ¹⁴⁵.

$\text{V}^{\text{IV}}\text{OL}_2$ complexes have been successfully proposed for antidiabetic treatment and, recently, as anticancer drugs.^{19, 39, 146} For example, bis(ethylmaltolato)oxidovanadium(IV), BEOV, arrived to phase IIa of the clinical trials.²⁴ Even if side effects emerged during this phase and the tests were stopped for the patent expiry,^{18, 24, 27} it and bis(maltolato)oxidovanadium(IV), BMOV, are the reference for new insulin-enhancing agents.^{25, 26} Today, an extensive research is devoted to the development of antitumor potential drugs, such as $[\text{V}^{\text{IV}}\text{O}(\text{Me}_2\text{phen})_2(\text{SO}_4)]^\ddagger$ and $[\text{V}^{\text{IV}}\text{O}(\text{flavonoidato})_2]$.^{16, 147, 148, 149} The main advantage of working with $\text{V}^{\text{IV}}\text{OL}_2$ lies in the possibility to fine tune the drug properties acting on the chelating functional groups to minimize toxicity, increase stability and absorption in the gastrointestinal tract, control ligand exchange during the bloodstream transport, optimize the cellular uptake modeling the second coordination sphere interactions, and modulate liability for degradation and re-functionalization within the cell.

In a series of recent works based on the multistep combination of ESI-MS, EPR, full DFT and docking, we fully characterized the interaction several $\text{V}^{\text{IV}}\text{OL}_2$ ($L = \text{dhp}$, L-mimosinato (mim), maltolato (ma), acetylacetonato (acac), pipemidato (pip), and 8-hydroxyquinoline-5-sulfonato ligand (hqs)[‡]) with Mb, Ub and Lyz.^{40, 54, 144, 145, 150} The potential anticancer and antidiabetic $[\text{V}^{\text{IV}}\text{O}(\text{dhp})_2]^\ddagger$ compound^{151, 152} will be presented as a first showcase for these interactions.

In the pH range 5-8, the 1:2 complex is in equilibrium between the $[\text{V}^{\text{IV}}\text{O}(\text{dhp})_2]$ (square pyramidal) and *cis*- $[\text{V}^{\text{IV}}\text{O}(\text{dhp})_2(\text{H}_2\text{O})]$ (distorted octahedral).^{153, 154} The deconvoluted ESI-MS spectrum measured on the system $[\text{VO}(\text{dhp})_2]/\text{Mb}$ with a

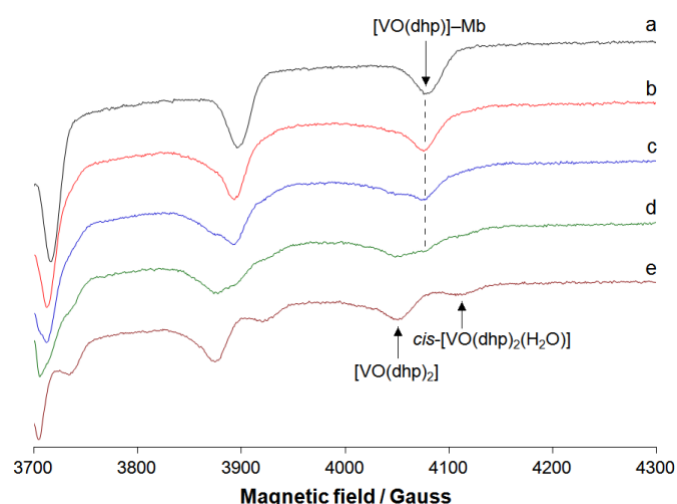


Fig. 9 High field region of the X-band anisotropic EPR spectra recorded on frozen solutions (120 K) containing: a) $[\text{VO}(\text{dhp})_2]/\text{Melm}$ 1/2; b) $[\text{VO}(\text{dhp})_2]/\text{Mb}$ 1/1; c) $[\text{VO}(\text{dhp})_2]/\text{Mb}$ 2/1; d) $[\text{VO}(\text{dhp})_2]/\text{Mb}$ 4/1; e) $[\text{VO}(\text{dhp})_2]$. $\text{V}^{\text{VO}2+}$ concentration was 1.0×10^{-3} M. With the dotted line the $M_1 = 7/2$ resonances of the adducts $[\text{VO}(\text{dhp})_2]-\text{Mb}$ are indicated. Adapted from ref. 145.

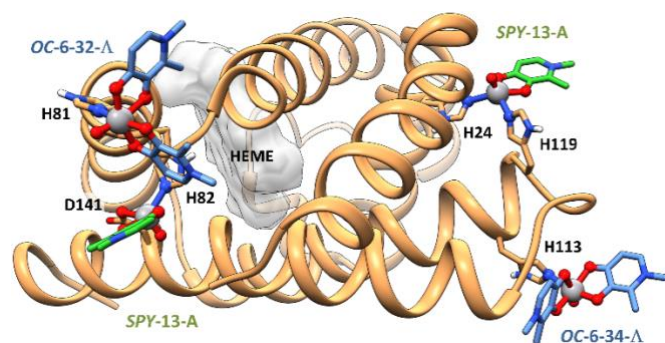
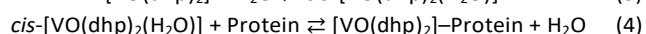
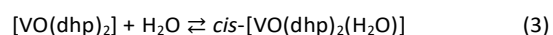


Fig. 10 Most stable adducts predicted by docking methods for the interaction of *cis*- $\text{VO}(\text{dhp})_2$ moiety with His 81 and His113, and $\text{VO}(\text{dhp})^+$ with (His24, His119) and (His82, Asp141) couples of donors of Mb. Adapted from ref. 145.

protein concentration of 5 μM and molar ratio 5/1 is reported in Fig. 8. The multiplex signals at 17858.0, 17997.1, 18202.1, and 18340.1 Da were attributed to the adducts $[\text{V}^{\text{VO}}(\text{dhp})]-\text{Mb}$, $[\text{V}^{\text{VO}}(\text{dhp})_2]-\text{Mb}$, $\{[\text{V}^{\text{VO}}(\text{dhp})] + [\text{V}^{\text{VO}}(\text{dhp})_2]-\text{Mb}\}$, and $2[\text{V}^{\text{VO}}(\text{dhp})_2]-\text{Mb}$, i.e. both the moieties $[\text{V}^{\text{VO}}(\text{dhp})]^+$ and $[\text{V}^{\text{VO}}(\text{dhp})_2]$ are able to bind Mb.

Anisotropic EPR spectra vary as a function of the ratio $\text{V}^{\text{VO}}(\text{dhp})_2/\text{Mb}$ (Fig. 9): at ratio 1/1 $[\text{VO}(\text{dhp})_2]-\text{Mb}$ is the major species in solution and its resonances coincide with those of *cis*- $[\text{VO}(\text{dhp})_2(\text{Melm})]$ with the equatorial 1-methylimidazole bound to V^{VO} . At ratios higher than 2/1 the absorptions of $[\text{V}^{\text{VO}}(\text{dhp})_2]$ and *cis*- $[\text{VO}(\text{dhp})_2(\text{H}_2\text{O})]$ appear and this means that the first two equivalents of *cis*- $\text{V}^{\text{VO}}(\text{dhp})_2$ find two His residues suitable for the metal coordination, forming the adduct $[\text{V}^{\text{VO}}(\text{dhp})_2]-\text{Mb}$ and $2[\text{V}^{\text{VO}}(\text{dhp})_2]-\text{Mb}$, in agreement with ESI-MS measurements:



At low $\text{V}^{\text{VO}}(\text{dhp})_2/\text{Mb}$ ratios the equilibria (3)-(4) are shifted to the right for the formation of the protein adduct, but increasing the ratio (4) shifts to the left with formation of $[\text{V}^{\text{VO}}(\text{dhp})_2]$ and

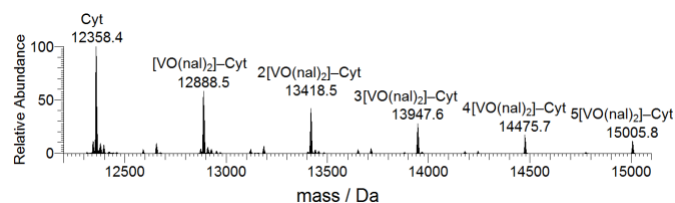


Fig. 11 Deconvoluted ESI-MS spectrum recorded on the systems containing: $[\text{V}^{\text{VO}}(\text{nal})_2(\text{H}_2\text{O})]$ and Cyt. The molar ratio V/Cyt was 5/1 and Cyt concentration 50 μM . Adapted from ref. 158.

cis- $[\text{V}^{\text{VO}}(\text{dhp})_2(\text{H}_2\text{O})]$ when protein binding sites are no longer available.

ESI-MS and EPR data were integrated by docking calculations on the eight enantiomers *OC*-6 of $[\text{V}^{\text{VO}}(\text{dhp})_2(\text{H}_2\text{O})]$. The Δ and Λ isomers *OC*-6-34, *OC*-6-34, *OC*-6-23 and *OC*-6-24 were optimized by DFT, the equatorial water was removed to allow the moiety *cis*- $\text{V}^{\text{VO}}(\text{dhp})_2$ to interact with Mb (PDB: 4DC8¹⁵⁵) using the force-field for vanadium.^{41, 54, 55} The candidate residues were identified through a relative Solvent Excluded Surface (SES) calculation that shows that the potential donors are His81, His113, His116, and His119. The results indicated that only His81 and His113 are able to interact with *cis*- $\text{V}^{\text{VO}}(\text{dhp})_2$ ($F_{\text{max}} = 45.3\text{-}49.4$ and $F_{\text{mean}} = 42.0\text{-}47.4$), Fig. 10. The binding of $\text{V}^{\text{VO}}(\text{dhp})^+$ moiety – suggested by ESI-MS – was also modelled by dockings: the enantiomers *SPY*-5-13-A and *SPY*-5-13-C were optimized by DFT methods, the two H_2O molecules removed and the two equatorial sites activated. Three potential sites were predicted with relative affinity order: (His24, His119) > (His82, Asp141) > (Glu83, Asp141), Fig. 10.

To summarize, ESI-MS allowed determining the number of moieties ($\text{V}^{\text{VO}}\text{OL}^+$ or $\text{V}^{\text{VO}}\text{OL}_2$) bound to protein, EPR to distinguish the type of residues involved in the coordination, DFT and docking to predict the specific residues involved in the V coordination as well as the 3D structure of the adducts.

As a second showcase, we describe a more complex system, formed by bis-chelated $\text{V}^{\text{VO}2+}$ species of nalidixato ligand (nal^+), *cis*- $[\text{V}^{\text{VO}}(\text{nal})_2(\text{H}_2\text{O})]$, with cytochrome *c* (Cyt), where both *coordinative* and *inert* binding are observed. Nalidixic acid belongs to the quinolones family, one of the most common among the antibacterials, which also aroused interest as organic ligands in the design of metal complexes with potential synergistic pharmacological activity. *Cis*- $[\text{V}^{\text{VO}}(\text{nal})_2(\text{H}_2\text{O})]$ was recently proved to be an antimicrobial stronger than the free ligand against several common bacteria, in particular when it is encapsulated into nanoparticles.¹⁵⁶

For this system, firstly the speciation in aqueous solution has been ascertained. EPR and ESI-MS measurements on the binary system $\text{V}^{\text{VO}2+}/\text{nal}$ 1:2 showed that, beside the presence of the mono-chelated species, an equilibrium between the penta-coordinated square pyramidal $[\text{V}^{\text{VO}}(\text{nal})_2]$ and the hexa-coordinated *cis*-octahedral *cis*- $[\text{V}^{\text{VO}}(\text{nal})_2(\text{H}_2\text{O})]$ exists.¹⁵⁷ DFT calculations of the energy stability and spin Hamiltonian parameters allowed to establish the most stable isomers in solution among the penta-coordinated *SPY*-5-(12,13) and hexa-coordinated *OC*-6-(23,24,32,34) species.¹⁵⁷

ESI-MS recorded on the ternary system *cis*- $[\text{V}^{\text{VO}}(\text{nal})_2(\text{H}_2\text{O})]/\text{Cyt}$ unveils up to five peaks corresponding to the adducts $n[\text{VO}(\text{nal})_2]-\text{Cyt}$ with $n = 1\text{-}5$ (Fig. 11).¹⁵⁸ The major finding of

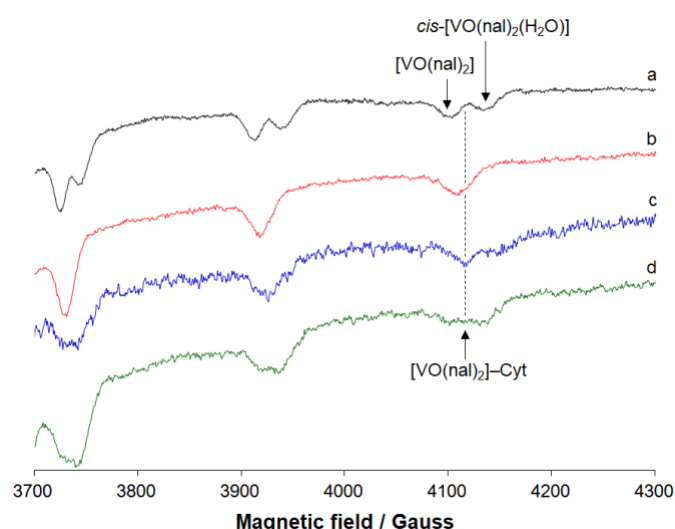


Fig. 12 High field region of the anisotropic EPR spectra recorded on frozen solutions (120 K) containing: a) $[\text{VO}(\text{nal})_2(\text{H}_2\text{O})]$; b) $[\text{VO}(\text{nal})_2(\text{H}_2\text{O})]/\text{MeIm}$ 1/2; c) $[\text{VO}(\text{nal})_2(\text{H}_2\text{O})]/\text{Cyt}$ 1/1 and d) $[\text{VO}(\text{nal})_2(\text{H}_2\text{O})]/\text{Cyt}$ 2/1. V^{VO} concentration was 5.0×10^{-4} M. With the dotted line the $M_I = 7/2$ resonances of the adducts $[\text{VO}(\text{nal})_2]-\text{Cyt}$ are indicated. Adapted from [ref. 158](#).

ESI-MS is the number of peaks of VCs–protein adducts and the challenge is to distinguish between strong *coordinative* interactions and weak non-specific *inert* bindings. The detection of the species involved in the *inert* interactions could be favoured in the gas phase after the solvent evaporation during the ionization process in the ESI chamber.¹⁵⁹

To obtain a first differentiation between *coordinative* and non-specific *inert* binding, EPR anisotropic spectra were recorded on the system $[\text{V}^{\text{VO}}(\text{nal})_2(\text{H}_2\text{O})]/\text{Cyt}$ with ratio 1/1 and 2/1 (Fig. 12). At ratio 1/1, the resonances can be attributed to an adduct $[\text{V}^{\text{VO}}(\text{nal})_2]-\text{Cyt}$ in which the fourth equatorial water molecule is replaced by an Asp/Glu-COO⁻ group, a donor weaker than the imidazole-N of $[\text{V}^{\text{VO}}(\text{nal})_2(\text{MeIm})]$ (A_2 is $170.3 \times 10^{-4} \text{ cm}^{-1}$ for $[\text{V}^{\text{VO}}(\text{nal})_2]-\text{Cyt}$ in the trace c vs. $169.1 \times 10^{-4} \text{ cm}^{-1}$ for $[\text{V}^{\text{VO}}(\text{nal})_2(\text{MeIm})]$ in the trace b of Fig. 12). Increasing the ratio $[\text{V}^{\text{VO}}(\text{nal})_2(\text{H}_2\text{O})]/\text{Cyt}$ to 2/1 (trace d of Fig. 12), the absorptions broaden and this can be ascribed to the contemporaneous presence of the two isomers of the 1:2 species $[\text{V}^{\text{VO}}(\text{nal})_2]$ and *cis*- $[\text{V}^{\text{VO}}(\text{nal})_2(\text{H}_2\text{O})]$ and to a second adduct $[\text{V}^{\text{VO}}(\text{nal})_2]-\text{Cyt}$, less stable than the first one revealed at ratio 1/1. Overall, the results indicate that only one or two $\text{V}^{\text{VO}}(\text{nal})_2$ equivalents bind to Cyt, while at ratios VC/Cyt higher than 2/1 the free 1:2 V^{VO} complexes are formed, which probably interacts with the protein surface through *inert binding*.

Therefore, joining the spectrometric and spectroscopic information, two *cis*- $\text{VO}(\text{nal})_2$ moieties interact through *coordinative* binding involving γ/δ -COO stemming from an Asp or Glu residue, and three additional equivalents bind Cyt in an *inert* manner on the protein surface.

Finally, by a series of dockings, the system has been fully characterized. The approach was as follows: i) with a first *coordinative* docking, the primary binding site has been determined and the adduct $[\text{V}^{\text{VO}}(\text{nal})_2]-\text{Cyt}$ identified; ii) a second *coordinative* docking was carried out on the structure $[\text{V}^{\text{VO}}(\text{nal})_2]-\text{Cyt}$ to identify the secondary site with a *coordinative* bond; iii) an additional *coordinative* docking has been performed on the structure $2[\text{V}^{\text{VO}}(\text{nal})_2]-\text{Cyt}$ without

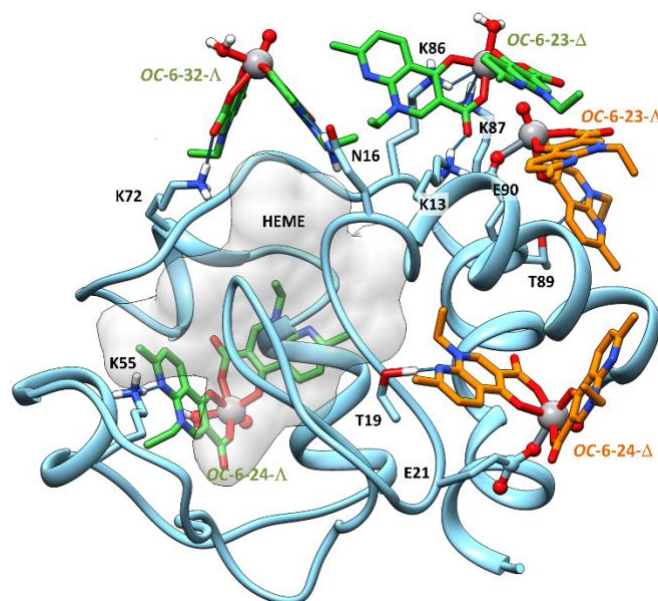


Fig. 13 Best docking solutions for the interaction of $[\text{VO}(\text{nal})_2]$ with Cyt to form the *coordinative* adduct $2[\text{VO}(\text{nal})_2]-\text{Cyt}$ (in orange), and best representative solutions of the first *cluster* for the non-specific *inert* interaction (in green). Adapted from [ref. 158](#).

finding another stable *coordinative* adduct; iv) at this point, a series of *non-covalent* dockings were performed on the adduct $2[\text{V}^{\text{VO}}(\text{nal})_2]-\text{Cyt}$ until reaching the total number of five moieties suggested by ESI.¹⁵⁸ Through these steps, a) Glu21 and Glu90 were identified as the best candidates to bind *OC-6-24-Δ* and *OC-6-23-Δ* isomers; b) the regions for the *inert* binding were predicted for *OC-6-32-Δ*, *OC-6-23-Δ* and *OC-6-24-Δ cis*-octahedral species and c) the secondary interactions stabilizing the $[\text{V}^{\text{VO}}(\text{nal})_2]-\text{Cyt}$ adducts were found (Fig. 13).

4.3 $\text{V}^{\text{III}}-\text{L}$, $\text{V}^{\text{IV}}-\text{L}$ and $\text{V}^{\text{VO}}-\text{L}$ potential drugs

The strategy illustrated in the previous sections can be pushed forward to characterize at molecular level the systems containing $\text{V}^{\text{III,IV,V}}-\text{L}$ and a protein. As an illustrative example $[\text{V}^{\text{VO}}(\text{acac})_2]$, one of the most studied VCs due to its anti-diabetic and antitumor effects,^{18, 19} will be illustrated. In this case, the interconversion between the three stable states +III, +IV and +V, possible under physiological conditions, can be discussed. In fact, $[\text{V}^{\text{VO}}(\text{acac})_2]$ could undergo reduction to $[\text{V}^{\text{III}}(\text{acac})_3]$ in the gastrointestinal tract and/or in the reducing cellular environment and oxidation to $[\text{V}^{\text{VO}_2}(\text{acac})_2]^-$ in the cell culture medium and partly in the blood serum. The results confirm the concept that, in the design of vanadium drugs, such biotransformation must be taken into account to identify the active species in the organism. To obtain a clear speciation profile of this VC in biological medium, ESI-MS and EPR data were collected for $[\text{V}^{\text{III}}(\text{acac})_3]$, $[\text{V}^{\text{VO}}(\text{acac})_2]$ and $[\text{V}^{\text{VO}_2}(\text{acac})_2]^-$ in aqueous solution as well as in the presence of Ub, Lyz and Mb.^{40, 144, 145} The data were integrated with computational (docking and QM) techniques. In the following paragraphs the results with Ub will be presented as an illustrative case.

ESI-MS spectrum recorded on an aqueous solution containing $\text{V}^{\text{III}}(\text{acac})_3$ shows the peaks of $[\text{V}^{\text{III}}(\text{acac})_3+\text{X}]^+$ and, with high intensity, $[\text{V}^{\text{VO}}(\text{acac})_2+\text{X}]^+$ with $\text{X} = \text{H}$ or Na .⁴⁰ On the binary

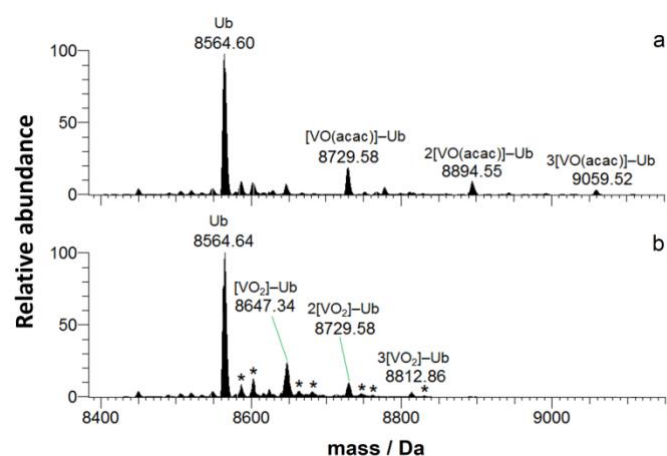


Fig. 14 Deconvoluted ESI-MS spectrum recorded on the systems containing: a) $V^{III}(acac)_3/Ub$ and b) $V^{VO_2}(acac)_2/Ub$. The molar ratio VC/Ub was 3/1 and Ub concentration 50 μM . With the asterisks the adducts with the binding of one and two water molecules are indicated. Adapted from ref. 40.

system $H_2V^{VO_4^-}/Hacac$ only the peaks relative to $[Hacac+X]^+$ and $[H_2V^{VO_4}]^-$ derived from the hydrolysis of $V^{VO_2}(acac)_2^-$ are detected confirming that vanadate(V) complexes are not or little stable in the order of μM concentration of V.¹⁶⁰ In contrast, on the system $V^{III}(acac)_3/Ub$, $V^{III}(acac)_3$ is quantitatively oxidized to V^{VO} and only the peaks of the adducts $n[V^{VO}(acac)]-Ub$ with $n = 1-3$, were detected (Fig. 14, a). Similarly to what observed in the binary system, working with $V^{VO_2}(acac)_2^-/Ub$ no traces of V^V complexes were observed and only the signals corresponding to the adducts $n[V^{VO_2}]-Ub$ with $n = 1-3$ were revealed (Fig. 14, b). EPR analysis on the biological systems confirms the one electron oxidation of V^{III} to V^{VO} and the contemporaneous presence of the adducts $n[V^{VO}(acac)]-Ub$, with A_2 compatible with one $acac^-$ ligand and two O-donors stemming from carboxylates (Asp and/or Glu) or carbonyl (backbone or Gln/Asn) or, alternatively, one His-N and one O-donor. The increase of concentration from μM to mM results in the formation of $[V^{VO}(acac)_2]$ which does not interact with proteins through *coordinative* nor *inert* binding. In the system with $V^{VO_2}(acac)_2^-$ the hydrolysis favours the dissociation of the complex, giving rise up to $3[V^{VO_2}]-Ub$ adducts.

The *in silico* prediction has been based on: i) the determination of the DFT minima in solution for $[V^{VO}(acac)_2]$, $[V^{VO}(acac)(H_2O)]^+$ and $[V^{VO_2}(H_2O)_3]^+$ to obtain the metal moieties that interact with protein; ii) the exploration of the structure of Ub, finding those regions containing the (Asp/Glu, Asp/Glu), (Asp/Glu, Asn/Gln) or (Asn/Gln, Asn/Gln) motifs able to bind the metal fragments; and iii) the docking of the vanadium moieties to Ub to gain a molecular view of the formed adducts.

At the end of the modelling, the amino acid donors coordinating $V^{VO}(acac)^+$ and $V^{VO_2}(H_2O)_n^+$ moieties were completely characterized: the binding sites with (Glu16, Glu18), (Glu24, Asp52), and (His68, H_2O) donors were predicted (Fig. 15). Their structure is stabilized by strong *H-bonds* between the $V=O$ group and side-chain $NH/NH_2/NH_3^+$ groups of Lys6, Arg42, Gln49, Arg54, His68, and Arg72. Finally, the absence of *inert* binding of $[V^{VO}(acac)_2]$ toward Ub has been confirmed by the scoring lower than that was recently established for a *rigid-limit*

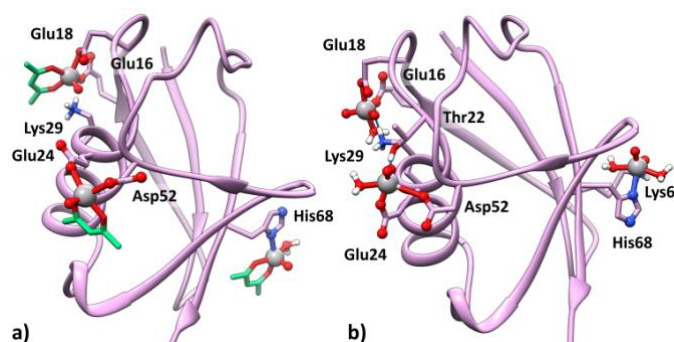


Fig. 15 Most stable structures predicted by docking for the adducts of V-acac species with Ub: a) $[V^{VO}(acac)]-Ub$ and b) $[V^{VO_2}(H_2O)_n]-Ub$, with $n = 1-2$. The hydrogen bonds are highlighted with the full blue lines. Adapted from ref. 40.

EPR spectrum (16-17, see Table 2) and by the presence of several clusters highlighting no specificity of the receptor. Overall, the results suggested that only $V^{VO}(acac)^+$ and $V^{VO_2}^+$ are the active species interacting with proteins at physiological conditions.

The showcases presented in this section highlight again that computational tools, carefully integrated with selected instrumental techniques, give biospeciation and structural insights, foundational for any novel drug design project and often precluded by the use of only experimental techniques.

4.4 V-enzymes

Predictive tools about enzymatic activity and inhibition are cornerstones in design of new drugs as well as *de novo* enzymes. In particular, the pharmacological activity of various metallodrugs could be based on the inhibition or activation of certain enzymatic processes as in the case of V-based antidiabetic drugs. In fact, vanadate(V)²² and oxidovanadium(IV)²³ inorganic species exert their insulin-mimetic activity either inhibiting intracellular PTP-1B or activating cyt-PTK leading to the signal transduction cascade for glucose uptake. As an example the inhibition of phosphatases by $V^{VO_4}{}^{3-}$ is explained by its structural similarity with $PO_4}{}^{3-}$, making vanadate(V) indistinguishable in the molecular recognition.^{129, 161} However, for $PO_4}{}^{3-}$ the pentavalent form is only a transition state achieved after the binding to the active site, while $V^{VO_4}{}^{3-}$ forms stable penta-coordinated adducts, resulting in a strong inhibition. On the other hand, the same phosphatase inhibition is the basis of the phytase-vanadate ArMs for which $V^{VO_4}{}^{3-}$ binds to the phosphate native site. In this scenario, we recently studied at the molecular level the binding of $V^{VO_2}{}^{2+}$ in VBrPO and IGPD.

Upon reduction by dithionite of the V^V centre of VBrPO to V^{IV} , its activity drastically decreases. EPR data show a value of $A_2(^{51}V)^{exptl}$ of $167.5 \times 10^{-4} \text{ cm}^{-1}$ and $160.1 \times 10^{-4} \text{ cm}^{-1}$ at pH 4.2 and 8.4, respectively suggesting the binding of some His residues.¹⁶² $A_{iso}(^{14}N)^{calcd}$ of 3.1 and 5.3 MHz observed in the ESEEM spectrum confirms the presence of a His-N in the equatorial plane.¹⁶³ Docking studies followed by full DFT cluster optimization suggest a unique binding site coincident to the catalytic one, with coordination of Ser416 (axial), His418 and His486 in *trans* to each other and a water molecule completing the

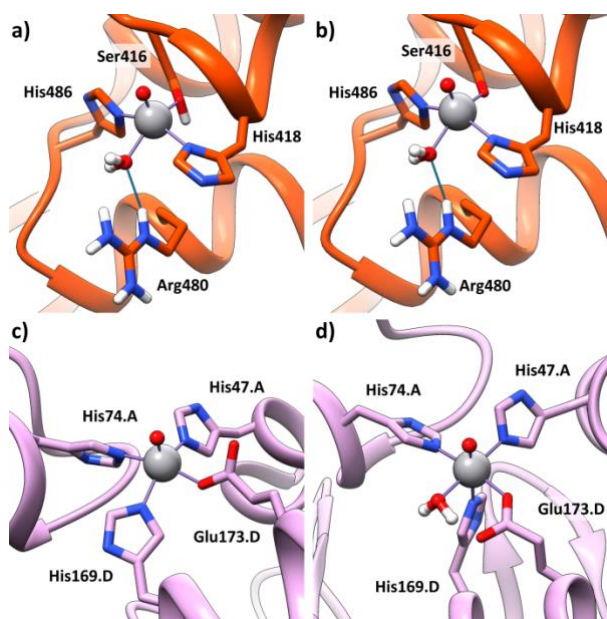


Fig. 16 DFT refined structures of the $V^{IV}O^{2+}$ sites in: a) VBrPO at pH 4.2; b) VBrPO at pH 8.4; c) IGPD mode α ; and d) IGPD mode β . Adapted from ref. 164.

coordination sphere (Fig. 16).¹⁶⁴ However, at different pH three binding modes are possible considering that both Ser416 and the fourth equatorial H_2O could be deprotonated. To shed light on the protonation state, subsequent ΔE_{bind} and spin Hamiltonian parameters simulations have been carried out allowing to rationalize the EPR data as a function of pH. At low pH, when Ser and His are partially protonated, the coordination set results (Ser416-OH, His418-N, His486-N; H_2O) giving the large value of $A_z(^{51}V)^{exptl}$ (Fig. 16, a), while at high pH the complete deprotonation of the side-chains leads to the motif (Ser416-O⁻, His418-N, His486-N; H_2O) with a lowering of $A_z(^{51}V)^{exptl}$ (Fig. 16, b).¹⁶⁴ The possibility of simultaneous deprotonation of both Ser416 and H_2O was discarded, considering the $A_{iso}(^{14}N)^{calcd}$ of 6.9 and 7.3 MHz, significantly different from the experimental values.

The binding of $V^{IV}O^{2+}$ to the apo-IGPD, a Mn^{II} -dependent enzyme,¹⁶⁵ was used as spin probe to explore the metal environment,¹⁶⁶ a common application of V^{IV} species. The X-band EPR spectrum of $V^{IV}O^{2+}$ -IGPD showed three resonances at increasing pH (α , β and γ) indicating different coordination environments, with $A_z(^{51}V)^{exptl}$ of 169.1, 161.6 and $140.6 \times 10^{-4} \text{ cm}^{-1}$, respectively.¹⁶⁶ $A_z(^{51}V)^{exptl}$ values for sites α and β suggest the involvement of His-N donors, while for site γ stronger donors are expected. $A_{iso}(^{14}N)^{exptl}$ of 7.0 MHz measured by ESEEM confirms these findings.¹⁶⁶ A first docking analysis found several possible binding modes with comparable affinity and population. The analysis of the full DFT binding energies and EPR/ESEEM simulated parameters allowed defining two modes as the best candidates for resonances α and β (Fig. 16, c and d), while no coincidence was found for site γ with an extremely low value of $A_z(^{51}V)^{exptl}$.¹⁶⁴ The site α corresponds to the motif (His47, His74, His170, Glu173) with $A_z(^{51}V)^{calcd} = 166.8 \times 10^{-4} \text{ cm}^{-1}$; site β to (His73, His145(ax), His170, Glu77; H_2O) with $A_z(^{51}V)^{calcd} = 164.3 \times 10^{-4} \text{ cm}^{-1}$. The resonance below 2.5 MHz in

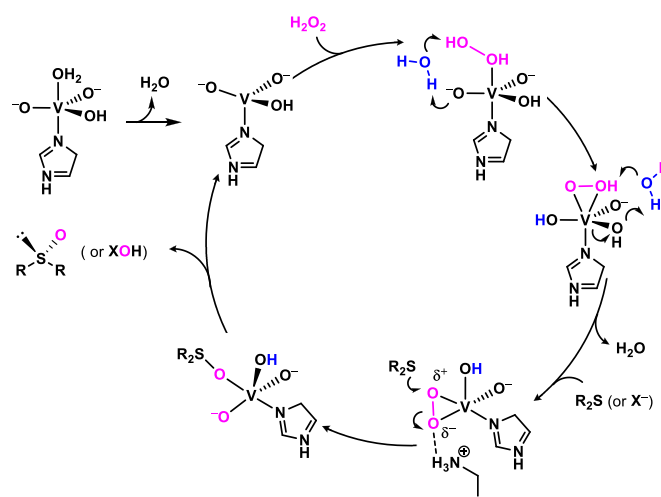


Fig. 17 Catalytic cycle for oxidation of halides and sulfoxidation of sulphides by VHOPOs like enzymes. Adapted from refs. 29, 172 and 173.

the ESEEM signals further support these assignment ($A_{iso}(^{14}N)^{calcd}$ is 0.5 MHz for both the sites α and β).

Overall, these results highlight that His-N and Asp/Glu-COO⁻ are the most affine donors for V^{IV} ,¹⁵⁸ however, the binding of deprotonated Ser residues is also possible.

4.5 V-based *de novo* enzymes

Since its discovery, vanadium attracted attention in homogeneous catalysis. This is due to its relative low toxicity and high availability, the accessibility to catalytically relevant forms using green oxidants (O_2 , air or H_2O_2), the easy interconversion between its stable oxidation states (+II, +III, +IV and +V) and its large variety of coordination number (up to 8). V-based homogeneous catalysts demonstrated high efficiency in epoxidations, sulfoxidations, haloperoxidations, C–C bond, Mannich-type processes, polymerizations and bond cleavage, including asymmetric and stereoselective processes.^{29, 30, 31} Moreover, the presence of vanadium in natural biocatalysis, such in haloperoxidases (HPOs) and nitrogenases,⁴⁵ makes vanadium a perfect candidate to be incorporated in artificial metalloenzyme.

In late '90 of the past century, taking advantage of enzyme promiscuity, several groups expanded the activity of VHOPOs toward asymmetric sulfoxidation. Allenmark *et al.* achieved up to 91% enantiomeric excess (ee) using V-bromoperoxidase (VBrPO) from the alga *Corallina officinalis*.³² Comparable ee was reached by Wever group using VBrPO from different seaweed sources.³³ However, this method limits the substrate scope.³⁷ Taking advantage of VCs binding properties, a more promising approach was used by Sheldon *et al.* incorporating vanadate(V) in the biological scaffold of several proteins (albumin, apoferritin, phytases, acid phosphatase, phospholipase D, aminoacylase, sulfatase) giving rise to a wide range of semisynthetic ArMs.³⁵ The highest success in terms of yield, turnover and selectivity has been reached with the phytases class of peroxidases;^{34, 35, 36} particularly, vanadate(V)-loaded *Aspergillus ficuum* phytase led to a phytase-vanadate ArMs that catalyzes sulfoxidation of sulfides with promising

enantioselectivity (66%).¹⁶⁷ Further improvements of catalytic properties for asymmetric sulfoxidation as well as the expansion towards other substrates and reaction types, require a novel rational design based on a deep understanding of the factors governing the processes.

The active site of phytase is structurally similar to that of acid phosphatase and V-chloroperoxydase (VCIPO), suggesting a similar environment with the axial coordination of V^{VO}_4 moiety by a His-N plus secondary stabilization through *H-bond* with His404, Lys353 and two arginine side-chains, Arg360 and Arg490. Mechanistic hypotheses also pointed out similarity with VCIPOs, with the sulphide entailing a nucleophilic attack toward the side-on coordinated peroxide in an asymmetric manner favoured by the secondary interactions and hindrance exerted by the protein scaffold toward the substrate.³⁴ However, neither 3D structures nor complete mechanistic studies of V^{VO}_4 -phytase have been reached so far and a clear picture of the enzymatic catalysis is still elusive.

In a first attempt to rationalize the biocatalysis of VCIPO, taking advantage of the X-ray structure of both resting and peroxo intermediates, Pecoraro and De Gioia investigated the formation of the peroxo complex by means of DFT using the model catalyst $[V^{VO}_2(OH)_2(Im)]^-$, where Im is imidazole.¹⁶⁸ Their results highlighted that the protonation of $[V^{VO}_2(OH)_2(Im)]^-$ to give $[V^{VO}_2(OH)(OH)_2(Im)]$ is the first step leading to the activated cofactor with a water molecule in the apical position. The second step is the replacement of water by H_2O_2 through a dissociative pathway giving rise first to the side-on hydroperoxo species $[V^{VO}_2(H_2O_2)(OH)(Im)]$, with an energy barrier about 7 kcal mol⁻¹, that – in its turn – evolves in a practically barrierless process to the side-on peroxo active catalyst $[VO(OH)(O)_2(Im)]$. For the step entailing the conversion of the hydroperoxo- to peroxo-intermediate, a series of water mediated proton-transfers have been invoked, pointing out that the presence of species acting as proton shuttles significantly decreases the kinetic of the process (Fig. 17). In a subsequent study, Gascón *et al.* integrated already reported ⁵¹V NMR, UV-Vis with full atom QM/MM study, providing further insight onto the protonation of the resting state.¹⁶⁹ In that work, the experimental ⁵¹V chemical shifts (δ_{iso}) and excitation wavelength (λ_{max}) have been compared with the computed parameters for a series of eight different protonation states. As a conclusion, it was confirmed that the protonation state displaying an apical H_2O leads to the smallest deviations ($\Delta\delta_{iso}$ and $\Delta\lambda_{max}$) as well as the lowest energy of the series, highlighting also the fundamental role of His404 in the stabilization of the activated cofactor. A recent QM/MM study pointed toward the same direction, although in those simulations the *H-bond* is mediated by an additional water, $V-OH_2\cdots OH_2\cdots N-His$.¹⁷⁰ Moreover, in the same work with Natural Bond Orbital (NBO) and Atoms-In-Molecules (AIM) approaches, additional *H-bonds* between the oxo ligands and Lys353, Arg360 and Arg490 have been highlighted, suggesting their role in enhancing the rate of catalysis. The *H-bond* with Lys353 seems to be an important factor for polarize the peroxo group, in fact the mutation Lys353Ala resulted in a considerably reduction of the catalytic efficiency.¹⁷¹ Pecoraro and De Gioia first,¹⁷² and Pacios and Gálvez afterward,¹⁷³ with QM cluster methods

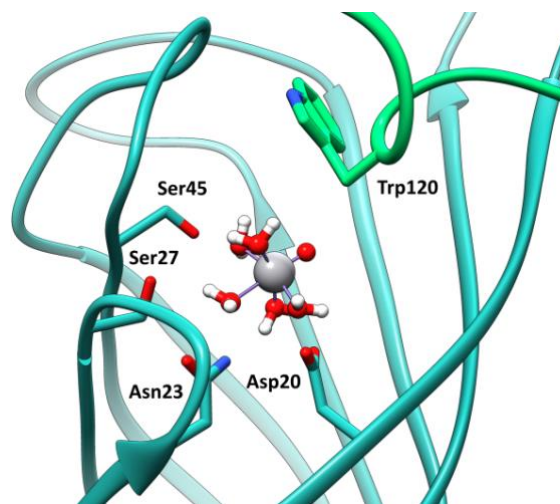


Fig. 18 Modelled structure of $V^{VO}(H_2O)_5$ -Sav. Interacting residues are shown in stick representation. In green Trp120 from monomer D, which closes the biotin pocket, is indicated. Adapted from ref. 38.

completed the cycle for the chlorination, bromination, sulfoxidation and iodination reaction of VHPOs. From the end-on peroxo intermediate a nucleophilic attack by X^- or RSR on the polarized pseudo-axial oxo, with concomitant O–O breaking in a SN_2 like mechanism, leads to a penta-coordinated trigonal bipyramid. The energy barriers associated to the process, when computed in presence of Lys353 model and using continuum model for simulating the protein scaffold, result in the range of 8.5–17.4 kcal mol⁻¹, making the process quite affordable. From the trigonal bipyramidal intermediate, axial O protonation and IOH substitution by H_2O follow in a barrierless manners, closing the cycle and recovering the catalytic four-coordinated species (Fig. 17).

The limited structural and mechanistic studies on V-based enzymes, particularly for asymmetric processes, should be considered one of the main reasons behind the little progress in the field. In fact, in the context of *de novo* design of V-based ArMs, a unique example was reported so far by Ward and coworkers incorporating oxidovanadium(IV) into the streptavidin (Sav) scaffold.³⁸ The novel hybrid catalyst displayed excellent performances in terms of ee and conversion in the asymmetric oxidation of alkyl, dialkyl and aryl sulfides in the presence of *t*-BuOOH as an oxidant. Structural and mechanistic insights have been obtained by the integrated application of EPR, modification of the reaction conditions, mutation experiments and molecular docking, proving the $V^{VO}2^+$ *inert binding* at the biotin site. EPR analysis of the binary system $V^{VO}2^+$ -Sav shows a value of HFC A_z of 182×10^{-4} cm⁻¹ coincident to that for the aquaion recorded in aqueous solution, demonstrating the absence of coordination by donors stronger than water-O, and suggesting an *inert binding*. Performing the reaction with an excess of biotin resulted in the racemic product, while using biotin-free Sav led up to 93% of selectivity and quantitative conversion, indicating that $V^{VO}2^+$ binds the same pocket of biotin. Docking analysis focused on the biotin pocket using the DFT minimum of $[V^{VO}(H_2O)_5]^{2+}$ as metallo-ligand showed a clear interaction of the moiety sharing similar *H-bond* network by Asp128, Asn23, Ser27, Ser45 displayed by

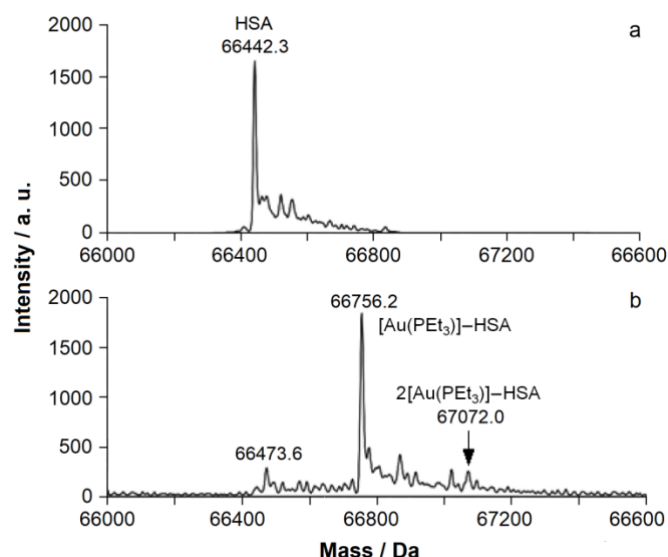


Fig. 19 Deconvoluted ESI-MS TOF spectra recorded on the systems containing: a) HSA and b) $[\text{Au}(\text{PEt}_3)]^+/\text{HSA}$ 1.33/1. Adapted from ref. 182

biotin (Fig. 18). The model was refined by MD simulation confirming the stability of the adduct, as well as the retention of the secondary interaction network along the whole trajectory of 6 ns. Finally, mutation of the Asp128 to Ala resulted in a total loss of stereoselectivity, supporting the biotin pocket as the active site and Asp128 as one of the main factor of the observed ee. Interestingly, using bulkier sulfide substituents increased the ee, highlighting the role of proper substrate dispositions in the active site for efficient selectivity. Future V-based ArMs design strategies should be built on top of the information given by these integrated studies rationally handling either the catalytic center or introducing the proper interactions in the second coordination sphere to control both stereo- and regioselectivity.

5. Generalization to other MCs

The proposed integrated experimental/computational approach is applicable to a wide ensemble of metallodrug–protein/peptide systems or to metal based cofactors–ArMs for which no structural data are available. Recent applications are the binding elucidation of Pt- and Ru-based metallodrugs in proteins as well as the Cu- and Mn-based cofactors in artificial metalloenzymes.^{9, 174, 175, 176}

In the field of metallodrug design, the binding sites of antiarthritic Auranofin and other cytotoxic gold compounds under experimentation share the same structural motif and $[\text{Au}(\text{PEt}_3)]^+$ moiety has released in aqueous solution.^{177, 178, 179} HSA is the protein candidate to transport Au(I) species in a human organism, even though no X-ray determinations are reported for the adducts between the $[\text{Au}(\text{PEt}_3)]^+$ moiety and HSA. The system can be fully characterized by an integrated approach in which EPR is replaced by NMR suitable for diamagnetic species. The major peak in the ESI-MS TOF spectra at 66756.2 Da is attributed to $[\text{Au}(\text{PEt}_3)]\text{-HSA}$, while another peak at 67072.0 Da could be assigned to $2[\text{Au}(\text{PEt}_3)]\text{-HSA}$, with

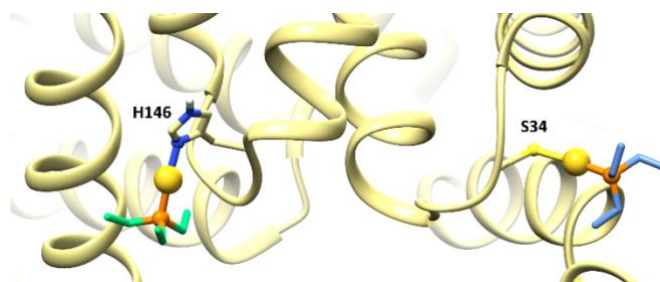


Fig. 20 The two binding sites proposed by docking calculations for interaction of $[\text{Au}(\text{PEt}_3)]^+$ moiety to HSA. The primary binding site with Cys34 (on the right) and the secondary binding site with His146 (on the left) were shown. Adapted from ref. 41.

two fragments bound to different residues (Fig 19). ^1H NMR spectra suggested that the binding of Cys34- S^- to Au^{I} causes a movement of Cys34 residue from a buried to an exposed environment which – in its turn – is coupled to a motion of His3 in the N-terminal region of the domain IA of albumin.¹⁸⁰

Therefore, based on MS and ^1H NMR evidence, it was concluded that Cys34 is the first residue interacting with $[\text{Au}(\text{PEt}_3)]^+$ fragment.^{180, 181, 182} Auratation of Cys34 has been recently reported by X-ray crystallography,¹⁸³ as well as further evidences of the affinity of Auranofin toward thiols.^{184, 185}

Docking studies, integrating spectroscopic/spectrometric data, allow to confirm this binding with $F_{\text{max}} = 41.8$ (Fig. 20). Interestingly, dockings suggest another interacting site, His146 with $F_{\text{max}} = 31.4$, located in the hydrophobic region of the protein (Fig. 20), and this second adduct would account for the species $2[\text{Au}(\text{PEt}_3)]\text{-HSA}$ revealed in the ESI-MS spectra.¹⁸² Notably, this finding is in line with the results of Sadler and co-workers for cyclophilin which – despite the four Cys in its structure – would bind $[\text{Au}(\text{PEt}_3)]^+$ with His133.¹⁸⁶

In a second example of integrated study, the binding sites and modes of oxaliplatin to insulin have been characterized by the integration of ESI-MS reported data with a multilevel docking, MD and QM/MM strategy.¹⁷⁴ Oxaliplatin, containing the labile dianionic oxalato ligand, in the bloodstream gives $[\text{Pt}(\text{dach})]^{2+}$ or hydrolysis products like $[\text{Pt}(\text{dach})(\text{OH})]^+$, with two or one coordination vacancies with which serum bioligands could interact. This phenomenon has been pointed out to be responsible of off-target interactions. Insulin is one of the potential off-targets for Pt-drugs since it is involved in bioavailability reduction and might also determine resistance in certain cancer lines. By a preliminary docking assay three binding sites compatible with the experimental data have been characterized, and – upon MD relaxation – the QM/MM structures and binding energy have been obtained (Fig. 21). The primary binding mode (Fig 21, a) could facilitate the reduction of a disulphide bridge inducing a conformational change of insulin with potential effects on its biological functions (Fig 21, b). Moreover, in the same work, it was confirmed the potential simultaneous binding to insulin of two Pt^{II} moieties, $[\text{Pt}(\text{dach})]^{2+}$ and $[\text{Pt}(\text{dach})(\text{OH})]^+$, as suggested in the literature by ESI-MS based techniques (Fig 21, a).¹⁷⁴

Similar integration between coordination dockings, MDs and spectroscopy have been recently applied for the study of the interaction of $[\text{Ru}(\eta^6\text{-p-cymene})\text{Cl}_2(\text{L})]$ potential metallodrugs, where L is an isothiazole ligand, to calf thymus deoxyribonucleic

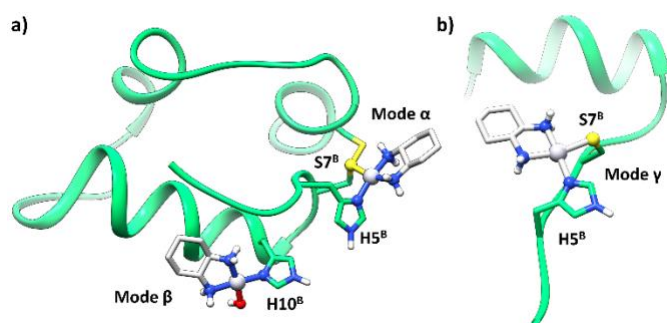


Fig. 21 QM/MM optimized structures of the α , β , and γ binding modes for the interaction of $[\text{Pt}(\text{dach})]^{2+}$ and $[\text{Pt}(\text{dach})(\text{OH})]^+$ moieties with insulin. Adapted from ref. 174

acid (CT-DNA) and HSA.¹⁷⁵ The modelling ascertained the coordination of Ru to N(7)dG7 of CT-DNA and Glu292 of HSA, that remembers the binding of $[\text{Ru}^{\text{II}}(1,4,7\text{-trithiacyclononane})(\text{ethylenediamine})\text{Cl}]^+$ to lysozyme through the side-chain of Asp101 and to proteinase K through Asp200 or Asp260, which replace the released chloride ligand.¹⁸⁷ The results supported the affinity of these potential drugs either toward CT-DNA major groove or IIa subdomain of HSA.

The integrated strategy here presented has been also applied in the field of artificial metalloenzymes design, particularly to a specific homodimer variant, A3, of the α Rep family of artificial repeat proteins.^{188, 189} The interest of this scaffold relies on the stability of its interdomain cavity and in the possibility to express the protein as a single chain bidomain metalloenzymes, offering the opportunity to selectively link a co-factor to one of its mutated subunits (A3'). In two subsequent works the 1:1 covalent anchoring of Cu(II)-phenanthroline, Cu(II)-terpyridine, and Mn(III)-tetraphenylporphyrin by a single mutation have been explored and their catalytic activity rationalized by means of instrumental/computational integration, suggesting the key factors of both selectivity and activation mechanisms of the ArMs.^{9, 176}

6. Conclusions

This review provided with major proof of concept evidence on the power of integrated instrumental data with MM and QM based computation either for metallodrugs or ArMs design with particular emphasis on vanadium systems.

The primary focus was on the recent expansion of protein-*ligand* dockings towards the inorganic world. After generated new scoring functions optimized for metal ions and metallo-*ligands*, the approach was validated on several structures formed by main group- and transition metal-containing *ligands* with various coordination numbers, geometries, and accessible coordination sites. Since the basis of the scoring function is to adapt *H-bond* terms to simulate coordination bonds, this approach is virtually adaptable to almost all docking programs. A second focus was to illustrate the efforts made for bridging computation with EPR and ESI-MS, two methods that provide insight on the interaction of metals with proteins but do not provide full three dimensional resolution of the entire system. Indeed, dealing with paramagnetic V^{IV} compounds, EPR gives information about the nature of the equatorial donors of the

complexes, while ESI-MS on the number and stoichiometry of the metal-protein adducts formed, beside the speciation in solution.

The relevance of the results obtained integrating experimental and computational information clearly opens the way not only for a rational design of new vanadium and metal based pharmacologically active compounds but also for the development of a vast number of fields in bioinorganic chemistry. This is actually what is proven in the showcases presented on V-based ArMs design, highlighting how a complete molecular knowledge offers the opportunity to design novel ArMs or improve known enzymes for new reactions.

The series of works discussed in this review highlights the manifold and multivariable nature of V species binding, which depends on: i) the conformation of the protein; ii) the stability and geometry of the complexes; iii) the ability of the chelating ligand to establish secondary interactions with the protein scaffold. The knowledge of binding sites and motifs opens the way for a rational design of specific guests modulating either their possibility to form *H-bonds* or van der Waals contacts with the host scaffold, or favouring asymmetric catalysis by mutating the environment.

The combined approach described for V species is completely generalizable toward systems containing different metals using other spectroscopic techniques in dependence of the metal features, such as NMR or UV-Vis for diamagnetic systems. The computational techniques described can be also applied to any metal species using the new series of metal force constants implemented recently into the GOLD framework or improving the opportune parameters for the specific system under analysis. To highlight the importance of integrating experimental/instrumental and computational techniques in the study of metal-protein and, in general, chemical systems, we conclude this review paraphrasing a famous Einstein's sentence: "*Experiment without computation is lame, computation without experiment is blind*".¹⁹⁰

Conflict of interest

There are no conflicts of interest.

Acknowledgements

G.S. and E.G. thank Regione Autonoma della Sardegna (grant RASSR79857) and Università di Sassari (fondo di Ateneo per la ricerca 2020); G.S. and J.-D.M. MINECO (grant CTQ2017-87889-P) and Generalitat de Catalunya (2017SGR1323) for the financial support.

Notes and references

- # In docking terminology the chemical moiety interacting with the protein is named ligand. This term could cause confusion when the ligand is a metal complex. Therefore, when it refers to the terminology used in the docking studies, it is written in italic in the text.

- ‡ Abbreviation for ligands: picolinato(−), pic; quercetinato(2−), que; morinato(−), mor; 7,8-dihydroxyflavonato(2−), 7,8-dhf; chrysinato(−), chr; 5-hydroxyflavonato(−), 5-hf; catecholato(2−), cat; 4,7-dimethyl-1,10-phenanthroline, Me₂phen; 1,2-dimethyl-3-hydroxy-4(1*H*)-pyridinonato, dhp(−); L-mimosinato(−), mim; maltolato(−), ma; acetylacetonato(−), acac; pipemidato(−), pip; 8-hydroxyquinoline-5-sulfonato(2−), hqs; nalidixato(−), nal.
- L. Riccardi, V. Genna and M. De Vivo, Metal–ligand interactions in drug design, *Nat. Rev. Chem.*, 2018, **2**, 100–112.
 - P. Janoš, A. Spinello and A. Magistrato, All-atom simulations to studying metallodrugs/target interactions, *Curr. Opin. Chem. Biol.*, 2021, **61**, 1–8.
 - D. Loreto, G. Ferraro and A. Merlino, Protein-metallodrugs interactions: Effects on the overall protein structure and characterization of Au, Ru and Pt binding sites, *Int. J. Biol. Macromol.*, 2020, **163**, 970–976.
 - T. Marzo, G. Ferraro, A. Merlino and L. Messori, in *Encyclopedia of Inorganic and Bioinorganic Chemistry*, ed. R. A. Scott, 2020, pp. 1–17.
 - K. A. Doucette, K. N. Hassell and D. C. Crans, Selective speciation improves efficacy and lowers toxicity of platinum anticancer and vanadium antidiabetic drugs, *J. Inorg. Biochem.*, 2016, **165**, 56–70.
 - A. Levina, D. C. Crans and P. A. Lay, Speciation of metal drugs, supplements and toxins in media and bodily fluids controls in vitro activities, *Coord. Chem. Rev.*, 2017, **352**, 473–498.
 - T. Jakusch and T. Kiss, In vitro study of the antidiabetic behavior of vanadium compounds, *Coord. Chem. Rev.*, 2017, **351**, 118–126.
 - J. Costa Pessoa, E. Garribba, M. F. A. Santos and T. Santos-Silva, Vanadium and proteins: Uptake, transport, structure, activity and function, *Coord. Chem. Rev.*, 2015, **301–302**, 49–86.
 - K. Kariyawasam, T. Di Meo, F. Hammerer, M. Valerio-Lepiniec, G. Sciortino, J.-D. Maréchal, P. Minard, J.-P. Mahy, A. Urvoas and R. Ricoux, An Artificial Hemoprotein with Inducible Peroxidase- and Monooxygenase-Like Activities, *Chem.–Eur. J.*, 2020, **26**, 14929–14937.
 - J. Gómez-González, Y. Pérez, G. Sciortino, L. Roldan-Martín, J. Martínez-Costas, J.-D. Maréchal, I. Alfonso, M. Vázquez López and M. E. Vázquez, Dynamic Stereoselection of Peptide Helicates and Their Selective Labeling of DNA Replication Foci in Cells, *Angew. Chem., Int. Ed.*, DOI: 10.1002/ange.202013039.
 - J. Costa Pessoa and I. Tomaz, Transport of Therapeutic Vanadium and Ruthenium Complexes by Blood Plasma Components, *Curr. Med. Chem.*, 2010, **17**, 3701–3738.
 - D. Gambino, Potentiality of vanadium compounds as anti-parasitic agents, *Coord. Chem. Rev.*, 2011, **255**, 2193–2203.
 - D. Rehder, The potentiality of vanadium in medicinal applications, *Future Med. Chem.*, 2012, **4**, 1823–1837.
 - M. Aureliano and C. A. Ohlin, Decavanadate in vitro and in vivo effects: facts and opinions, *J. Inorg. Biochem.*, 2014, **137**, 123–130.
 - E. Kioseoglou, S. Petanidis, C. Gabriel and A. Salifoglou, The chemistry and biology of vanadium compounds in cancer therapeutics, *Coord. Chem. Rev.*, 2015, **301–302**, 87–105.
 - I. E. Leon, J. F. Cadavid-Vargas, A. L. Di Virgilio and S. B. Etcheverry, Vanadium, ruthenium and copper compounds: a new class of nonplatinum metallodrugs with anticancer activity, *Curr. Med. Chem.*, 2017, **24**, 112–148.
 - D. Rehder, Vanadium in health issues, *ChemTexts*, 2018, **4**, 20.
 - D. Crans, C. L. Yang, A. Haase and X. Yang, in *Metallo-Drugs: Development and Action of Anticancer Agents*, eds. A. Sigel, H. Sigel, E. Freisinger and R. K. O. Sigel, De Gruyter GmbH, Berlin, 2018, vol. 18, pp. 251–280.
 - D. C. Crans, L. Henry, G. Cardiff and B. I. Posner, in *Essential Metals in Medicine: Therapeutic Use and Toxicity of Metal Ions in the Clinic*, ed. P. L. Carver, De Gruyter GmbH, Berlin, 2019, pp. 203–230.
 - S. Treviño, A. Díaz, E. Sánchez-Lara, B. L. Sanchez-Gaytan, J. M. Perez-Aguilar and E. González-Vergara, Vanadium in Biological Action: Chemical, Pharmacological Aspects, and Metabolic Implications in Diabetes Mellitus, *Biol. Trace Elem. Res.*, 2019, **188**, 68–98.
 - D. Rehder, The potentiality of vanadium in medicinal applications, *Inorg. Chim. Acta*, 2020, **504**, 119445.
 - Y. Shechter and S. J. D. Karlish, Insulin-like stimulation of glucose oxidation in rat adipocytes by vanadyl (IV) ions, *Nature*, 1980, **284**, 556–558.
 - S. Ramanadham, J. J. Mongold, R. W. Brownsey, G. H. Cros and J. H. McNeill, Oral vanadyl sulfate in treatment of diabetes mellitus in rats, *Am. J. Physiol. Heart Circ. Physiol.*, 1989, **257**, H904–H911.
 - K. H. Thompson, J. Lichter, C. LeBel, M. C. Scaife, J. H. McNeill and C. Orvig, Vanadium treatment of type 2 diabetes: A view to the future, *J. Inorg. Biochem.*, 2009, **103**, 554–558.
 - K. H. Thompson, B. D. Liboiron, G. R. Hanson and C. Orvig, in *Medicinal Inorganic Chemistry*, American Chemical Society, 2005, vol. 903, pp. 384–399.
 - K. H. Thompson and C. Orvig, Vanadium in diabetes: 100 years from Phase 0 to Phase I, *J. Inorg. Biochem.*, 2006, **100**, 1925–1935.
 - T. Scior, J. A. Guevara-Garcia, Q.-T. Do, P. Bernard and S. Laufer, Why antidiabetic vanadium complexes are not in the pipeline of “big pharma” drug research? A critical review, *Curr. Med. Chem.*, 2016, **23**, 2874–2891.
 - F. Chen, T. Wang and N. Jiao, Recent Advances in Transition-Metal-Catalyzed Functionalization of Unstrained Carbon–Carbon Bonds, *Chem. Rev.*, 2014, **114**, 8613–8661.
 - S. Takizawa, H. Gröger and H. Sasai, Vanadium in Asymmetric Synthesis: Emerging Concepts in Catalyst Design and Applications, *Chem.–Eur. J.*, 2015, **21**, 8992–8997.
 - R. R. Langeslay, D. M. Kaphan, C. L. Marshall, P. C. Stair, A. P. Sattelberger and M. Delferro, Catalytic Applications of Vanadium: A Mechanistic Perspective, *Chem. Rev.*, 2019, **119**, 2128–2191.
 - H. Pellissier, Enantioselective vanadium-catalyzed transformations. An update, *Coord. Chem. Rev.*, 2020, **418**, 213395.
 - M. Andersson, A. Willetts and S. Allenmark, Asymmetric Sulfoxidation Catalyzed by a Vanadium-Containing Bromoperoxidase, *J. Org. Chem.*, 1997, **62**, 8455–8458.
 - H. B. ten Brink, A. Tuijnman, H. L. Dekker, W. Hemrika, Y. Izumi, T. Oshiro, H. E. Schoemaker and R. Wever, Enantioselective Sulfoxidation Catalyzed by Vanadium Haloperoxidases, *Inorg. Chem.*, 1998, **37**, 6780–6784.
 - F. van de Velde, L. Könemann, F. van Rantwijk and R. A. Sheldon, The rational design of semisynthetic peroxidases, *Biotechnol. Bioeng.*, 2000, **67**, 87–96.
 - F. van de Velde, I. W. C. E. Arends and R. A. Sheldon, Biocatalytic and biomimetic oxidations with vanadium, *J. Inorg. Biochem.*, 2000, **80**, 81–89.

36. F. van de Velde, I. W. C. E. Arends and R. A. Sheldon, Vanadium-catalysed enantioselective sulfoxidations: rational design of biocatalytic and biomimetic systems, *Top. Catal.*, 2000, **13**, 259.
37. I. Correia, S. Aksu, P. Adão, J. C. Pessoa, R. A. Sheldon and I. W. C. E. Arends, Vanadate substituted phytase: Immobilization, structural characterization and performance for sulfoxidations, *J. Inorg. Biochem.*, 2008, **102**, 318-329.
38. A. Pordea, M. Creus, J. Panek, C. Duboc, D. Mathis, M. Novic and T. R. Ward, Artificial Metalloenzyme for Enantioselective Sulfoxidation Based on Vanadyl-Loaded Streptavidin, *J. Am. Chem. Soc.*, 2008, **130**, 8085-8088.
39. J. Costa Pessoa, S. Etcheverry and D. Gambino, Vanadium compounds in medicine, *Coord. Chem. Rev.*, 2015, **301-302**, 24-48.
40. G. Sciortino, V. Ugone, D. Sanna, G. Lubinu, S. Ruggiu, J.-D. Maréchal and E. Garribba, Biospeciation of Potential Vanadium Drugs of Acetylacetonate in the Presence of Proteins, *Front. Chem.*, 2020, **8**, 345.
41. G. Sciortino, E. Garribba and J.-D. Maréchal, Validation and Applications of Protein-Ligand Docking Approaches Improved for Metalloligands with Multiple Vacant Sites, *Inorg. Chem.*, 2019, **58**, 294-306.
42. G. Sciortino, D. Sanna, V. Ugone, A. Lledós, J.-D. Maréchal and E. Garribba, Decoding Surface Interaction of V^{IV} Metallo drug Candidates with Lysozyme, *Inorg. Chem.*, 2018, **57**, 4456-4469.
43. W. Shi and M. R. Chance, Metalloproteomics: forward and reverse approaches in metalloprotein structural and functional characterization, *Curr. Opin. Chem. Biol.*, 2011, **15**, 144-148.
44. J. Ward, E. Ollmann, E. Maxey and L. A. Finney, in *Metalloproteins*, Springer, 2014, pp. 171-187.
45. D. Rehder, *Bioinorganic Vanadium Chemistry*, John Wiley & Sons, Ltd, Chichester, 2008.
46. C. G. Azevedo, I. Correia, M. M. C. dos Santos, M. F. A. Santos, T. Santos-Silva, J. Douth, L. Fernandes, H. M. Santos, J. L. Capelo and J. Costa Pessoa, Binding of vanadium to human serum transferrin - voltammetric and spectrometric studies, *J. Inorg. Biochem.*, 2018, **180**, 211-221.
47. I. Boukhobza and D. C. Crans, Application of HPLC to measure vanadium in environmental, biological and clinical matrices, *Arab. J. Chem.*, 2020, **13**, 1198-1228.
48. N. P. Farrell, Multi-platinum anti-cancer agents. Substitution-inert compounds for tumor selectivity and new targets, *Chem. Soc. Rev.*, 2015, **44**, 8773-8785.
49. M. Wenzel and A. Casini, Mass spectrometry as a powerful tool to study therapeutic metallo drugs speciation mechanisms: Current frontiers and perspectives, *Coord. Chem. Rev.*, 2017, **352**, 432-460.
50. V. Ugone, D. Sanna, G. Sciortino, D. C. Crans and E. Garribba, ESI-MS Study of the Interaction of Potential Oxidovanadium(IV) Drugs and Amavadin with Model Proteins, *Inorg. Chem.*, 2020, **59**, 9739-9755.
51. B. D. Liboiron, in *High Resolution EPR: Applications to Metalloenzymes and Metals in Medicine*, eds. L. Berliner and G. Hanson, Springer, New York, 2009, vol. 28, pp. 507-549.
52. S. C. Larsen and N. D. Chasteen, in *Metals in Biology: Applications of High-Resolution EPR to Metalloenzymes*, eds. G. Hanson and L. Berliner, Springer, New York, 2010, vol. 29, pp. 371-409.
53. D. Sanna, V. Pecoraro, G. Micera and E. Garribba, Application of DFT methods to the study of the coordination environment of the VO^{2+} ion in V proteins, *J. Biol. Inorg. Chem.*, 2012, **17**, 773-790.
54. G. Sciortino, D. Sanna, V. Ugone, G. Micera, A. Lledós, J.-D. Maréchal and E. Garribba, Elucidation of Binding Site and Chiral Specificity of Oxidovanadium Drugs with Lysozyme through Theoretical Calculations, *Inorg. Chem.*, 2017, **56**, 12938-12951.
55. G. Sciortino, J. Rodríguez-Guerra Pedregal, A. Lledós, E. Garribba and J.-D. Maréchal, Prediction of the interaction of metallic moieties with proteins: an update for protein-ligand docking techniques, *J. Comput. Chem.*, 2018, **39**, 42-51.
56. L. Alonso-Cotchico, J. Rodríguez-Guerra, A. Lledós and J.-D. Maréchal, Molecular Modeling for Artificial Metalloenzyme Design and Optimization, *Acc. Chem. Res.*, 2020, **53**, 896-905.
57. H. B. Gray, J. S. Valentine and E. I. Stiefel, *Biological inorganic chemistry: structure and reactivity*, University Science Books, 2007.
58. F. Neese, A critical evaluation of DFT, including time-dependent DFT, applied to bioinorganic chemistry, *J. Biol. Inorg. Chem.*, 2006, **11**, 702-711.
59. F. Neese, Quantum chemical calculations of spectroscopic properties of metalloproteins and model compounds: EPR and Mössbauer properties, *Curr. Opin. Chem. Biol.*, 2003, **7**, 125-135.
60. M. Medhavi, V. Ambarish Sharan and Shankaracharya, Tools for Predicting Metal Binding Sites in Protein: A Review, *Curr. Bioinf.*, 2011, **6**, 444-449.
61. P. Chaskar, V. Zoete and U. F. Röhrig, Toward On-The-Fly Quantum Mechanical/Molecular Mechanical (QM/MM) Docking: Development and Benchmark of a Scoring Function, *J. Chem. Inf. Model.*, 2014, **54**, 3137-3152.
62. P. Vidossich and A. Magistrato, QM/MM Molecular Dynamics Studies of Metal Binding Proteins, *Biomolecules*, 2014, **4**, 616-645.
63. F. Li, N. Wang, L. Lu and G. Zhu, Regioselective Hydration of Terminal Alkynes Catalyzed by a Neutral Gold(I) Complex [(IPr)AuCl] and One-Pot Synthesis of Optically Active Secondary Alcohols from Terminal Alkynes by the Combination of [(IPr)AuCl] and $Cp^*RhCl[(R,R)\text{-TsDPEN}]$, *J. Org. Chem.*, 2015, **80**, 3538-3546.
64. M. Akhter, Challenges in Docking: Mini Review, *JSM Chem.*, 2016, **4**, 1025.
65. G. B. Akcapinar and O. U. Sezerman, Computational approaches for *de novo* design and redesign of metal-binding sites on proteins, *Biosci. Rep.*, 2017, **37**, BSR20160179.
66. P. Li and K. M. Merz, Metal Ion Modeling Using Classical Mechanics, *Chem. Rev.*, 2017, **117**, 1564-1686.
67. F. Neese, Prediction of molecular properties and molecular spectroscopy with density functional theory: From fundamental theory to exchange-coupling, *Coord. Chem. Rev.*, 2009, **253**, 526-563.
68. F. Neese, Prediction of electron paramagnetic resonance g values using coupled perturbed Hartree-Fock and Kohn-Sham theory, *J. Chem. Phys.*, 2001, **115**, 11080-11096.
69. G. Micera and E. Garribba, The effect of the functional, basis set, and solvent in the simulation of the geometry and spectroscopic properties of $V^{IV}O^{2+}$ complexes. chemical and biological applications, *Int. J. Quantum Chem.*, 2012, **112**, 2486-2498.
70. D. Sanna, G. Sciortino, V. Ugone, G. Micera and E. Garribba, Nonoxido V^{IV} Complexes: Prediction of the EPR Spectrum and Electronic Structure of Simple Coordination Compounds and Amavadin, *Inorg. Chem.*, 2016, **55**, 7373-7387.
71. G. Sciortino, N. Lihi, T. Czine, J.-D. Maréchal, A. Lledós and E. Garribba, Accurate prediction of vertical electronic transitions

- of Ni(II) coordination compounds via time dependent density functional theory, *Int. J. Quantum Chem.*, 2018, **118**, e25655.
72. G. Sciortino, G. Lubinu, J.-D. Maréchal and E. Garribba, DFT Protocol for EPR Prediction of Paramagnetic Cu(II) Complexes and Application to Protein Binding Sites, *Magnetochemistry*, 2018, **4**, 55.
 73. G. Micera and E. Garribba, Is the Spin-Orbit Coupling Important in the Prediction of the ^{51}V Hyperfine Coupling Constants of $\text{V}^{\text{IV}}\text{O}^{2+}$ Species? ORCA Versus Gaussian Performance and Biological Applications, *J. Comput. Chem.*, 2011, **32**, 2822-2835.
 74. S. Agarwal and R. Mehrotra, An overview of Molecular Docking, *JSM Chem.*, 2016, **4**, 1024.
 75. I. A. Guedes, C. S. de Magalhães and L. E. Dardenne, Receptor–ligand molecular docking, *Biophys. Rev.*, 2014, **6**, 75-87.
 76. G. L. Warren, C. W. Andrews, A.-M. Capelli, B. Clarke, J. LaLonde, M. H. Lambert, M. Lindvall, N. Nevins, S. F. Semus, S. Senger, G. Tedesco, I. D. Wall, J. M. Woolven, C. E. Peishoff and M. S. Head, A Critical Assessment of Docking Programs and Scoring Functions, *J. Med. Chem.*, 2006, **49**, 5912-5931.
 77. S. F. Sousa, A. J. M. Ribeiro, J. T. S. Coimbra, R. P. P. Neves, S. A. Martins, N. S. H. N. Moorthy, P. A. Fernandes and M. J. Ramos, Protein-Ligand Docking in the New Millennium – A Retrospective of 10 Years in the Field, *Curr. Med. Chem.*, 2013, **20**, 2296-2314.
 78. N. S. Pagadala, K. Syed and J. Tuszynski, Software for molecular docking: a review, *Biophys. Rev.*, 2017, **9**, 91-102.
 79. R. A. Friesner, J. L. Banks, R. B. Murphy, T. A. Halgren, J. J. Klicic, D. T. Mainz, M. P. Repasky, E. H. Knoll, M. Shelley, J. K. Perry, D. E. Shaw, P. Francis and P. S. Shenkin, Glide: A New Approach for Rapid, Accurate Docking and Scoring. 1. Method and Assessment of Docking Accuracy, *J. Med. Chem.*, 2004, **47**, 1739-1749.
 80. G. M. Morris, R. Huey, W. Lindstrom, M. F. Sanner, R. K. Belew, D. S. Goodsell and A. J. Olson, AutoDock4 and AutoDockTools4: Automated Docking with Selective Receptor Flexibility, *J. Comput. Chem.*, 2009, **30**, 2785-2791.
 81. C. R. Corbeil, C. I. Williams and P. Labute, Variability in docking success rates due to dataset preparation, *J. Comput.-Aided Mol. Des.*, 2012, **26**, 775-786.
 82. A. N. Jain, Scoring Functions for Protein-Ligand Docking, *Curr. Protein Pept. Sci.*, 2006, **7**, 407-420.
 83. R. C. Glen, A fast empirical method for the calculation of molecular polarizability, *J. Comput.-Aided Mol. Des.*, 1994, **8**, 457-466.
 84. C. Scholz, S. Knorr, K. Hamacher and B. Schmidt, DOCKTITE—A Highly Versatile Step-by-Step Workflow for Covalent Docking and Virtual Screening in the Molecular Operating Environment, *J. Chem. Inf. Model.*, 2015, **55**, 398-406.
 85. S. A. Hayik, R. Dunbrack and K. M. Merz, Mixed Quantum Mechanics/Molecular Mechanics Scoring Function To Predict Protein–Ligand Binding Affinity, *J. Chem. Theory Comput.*, 2010, **6**, 3079-3091.
 86. K. Raha and K. M. Merz, Large-Scale Validation of a Quantum Mechanics Based Scoring Function: Predicting the Binding Affinity and the Binding Mode of a Diverse Set of Protein–Ligand Complexes, *J. Med. Chem.*, 2005, **48**, 4558-4575.
 87. V. M. Robles, E. Ortega-Carrasco, E. G. Fuentes, A. Lledós and J.-D. Maréchal, What can molecular modelling bring to the design of artificial inorganic cofactors?, *Faraday Discuss.*, 2011, **148**, 137-159.
 88. V. M. Robles, M. Dürrenberger, T. Heinisch, A. Lledós, T. Schirmer, T. R. Ward and J.-D. Maréchal, Structural, Kinetic, and Docking Studies of Artificial Imine Reductases Based on Biotin–Streptavidin Technology: An Induced Lock-and-Key Hypothesis, *J. Am. Chem. Soc.*, 2014, **136**, 15676-15683.
 89. E. Ortega-Carrasco, A. Lledós and J.-D. Maréchal, Assessing protein–ligand docking for the binding of organometallic compounds to proteins, *J. Comput. Chem.*, 2014, **35**, 192-198.
 90. G. Jones, P. Willett and R. C. Glen, Molecular recognition of receptor sites using a genetic algorithm with a description of desolvation, *J. Mol. Biol.*, 1995, **245**, 43-53.
 91. G. Sciortino, E. Garribba, J. R. G. Pedregal and J. D. Marechal, Simple Coordination Geometry Descriptors Allow to Accurately Predict Metal-Binding Sites in Proteins, *ACS Omega*, 2019, **4**, 3726-3731.
 92. J. Rodríguez-Guerra Pedregal, G. Sciortino, J. Guasp, M. Municoy and J.-D. Maréchal, GaudiMM: A modular multi-objective platform for molecular modeling, *J. Comput. Chem.*, 2017, **38**, 2118-2126.
 93. J.-E. Sánchez-Aparicio, L. Tiessler-Sala, L. Velasco-Carneros, L. Roldán-Martín, G. Sciortino and J.-D. Maréchal, BioMetAll: Identifying Metal-Binding Sites in Proteins from Backbone Preorganization, *J. Chem. Inf. Model.*, 2021, **61**, 311-323.
 94. A. Moulin, J. H. Bell, R. F. Pratt and D. Ringe, Inhibition of Chymotrypsin by a Complex of Ortho-Vanadate and Benzohydroxamic Acid: Structure of the Inert Complex and Its Mechanistic Interpretation, *Biochemistry*, 2007, **46**, 5982-5990.
 95. Y. Lindqvist, G. Schneider and P. Vihko, Crystal structures of rat acid phosphatase complexed with the transition-state analogs vanadate and molybdate, *Eur. J. Biochem.*, 1994, **221**, 139-142.
 96. K. M. Holtz, B. Stec and E. R. Kantrowitz, A Model of the Transition State in the Alkaline Phosphatase Reaction, *J. Biol. Chem.*, 1999, **274**, 8351-8354.
 97. T. A. S. Brandão, A. C. Hengge and S. J. Johnson, Insights into the Reaction of Protein-tyrosine Phosphatase 1B: Crystal Structures for Transition State Analogs of Both Catalytic Steps, *J. Biol. Chem.*, 2010, **285**, 15874-15883.
 98. M. F. A. Santos, I. Correia, A. R. Oliveira, E. Garribba, J. C. Pessoa and T. Santos-Silva, Vanadium Complexes as Prospective Therapeutics: Structural Characterization of a V^{IV} Lysozyme Adduct, *Eur. J. Inorg. Chem.*, 2014, 3293-3297.
 99. K. M. Davis, M. Altmyer, R. J. Martinie, I. Schaperdorth, C. Krebs, J. M. Bollinger and A. K. Boal, Structure of a Ferryl Mimic in the Archetypal Iron(II)- and 2-(Oxo)-glutarate-Dependent Dioxygenase, TauD, *Biochemistry*, 2019, **58**, 4218-4223.
 100. J. Rittle, M. J. Field, M. T. Green and F. A. Tezcan, An efficient, step-economical strategy for the design of functional metalloproteins, *Nature Chem.*, 2019, **11**, 434-441.
 101. S. C. Lovell, J. M. Word, J. S. Richardson and D. C. Richardson, The penultimate rotamer library, *Proteins: Struct., Funct., Bioinf.*, 2000, **40**, 389-408.
 102. G. Bianco, S. Forli, D. S. Goodsell and A. J. Olson, Covalent docking using autodock: Two-point attractor and flexible side chain methods, *Protein Sci.*, 2016, **25**, 295-301.
 103. K. E. Hevener, W. Zhao, D. M. Ball, K. Babaoglu, J. Qi, S. W. White and R. E. Lee, Validation of Molecular Docking Programs for Virtual Screening against Dihydropteroate Synthase, *J. Chem. Inf. Model.*, 2009, **49**, 444-460.
 104. S.-Y. Huang, S. Z. Grinter and X. Zou, Scoring functions and their evaluation methods for protein-ligand docking: recent

- advances and future directions, *Phys. Chem. Chem. Phys.*, 2010, **12**, 12899-12908.
105. M. M. Roessler and E. Salvadori, Principles and applications of EPR spectroscopy in the chemical sciences, *Chem. Soc. Rev.*, 2018, **47**, 2534-2553.
 106. M. D. E. Forbes, L. E. Jarocho, S. Sim and V. F. Tarasov, Time-resolved Electron Paramagnetic Resonance spectroscopy, *Adv. Phys. Org. Chem.*, 2013, **47**, 1-83.
 107. D. Sanna, V. Ugone, G. Micera and E. Garribba, Temperature and solvent structure dependence of VO²⁺ complexes of pyridine-N-oxide derivatives and their interaction with human serum transferrin, *Dalton Trans.*, 2012, **41**, 7304-7318.
 108. R. F. Campbell and J. H. Freed, Slow-motional ESR spectra for vanadyl complexes and their model dependence, *J. Phys. Chem.*, 1980, **84**, 2668-2680.
 109. M. L. Munzarová and M. Kaupp, A Density Functional Study of EPR Parameters for Vanadyl Complexes Containing Schiff Base Ligands, *J. Phys. Chem. B*, 2001, **105**, 12644-12652.
 110. F. Neese, Metal and ligand hyperfine couplings in transition metal complexes: The effect of spin-orbit coupling as studied by coupled perturbed Kohn-Sham theory, *J. Chem. Phys.*, 2003, **118**, 3939-3948.
 111. A. C. Saladino and S. C. Larsen, Density Functional Theory Calculations of the Electron Paramagnetic Resonance Parameters for VO²⁺ Complexes, *J. Phys. Chem. A*, 2003, **107**, 1872-1878.
 112. C. P. Aznar, Y. Deligiannakis, E. J. Tolis, T. Kabanos, M. Brynda and R. D. Britt, ESE-ENDOR Study and DFT Calculations on Oxovanadium Compounds: Effect of Axial Anionic Ligands on the ⁵¹V Nuclear Quadrupolar Coupling Constant, *J. Phys. Chem. A*, 2004, **108**, 4310-4321.
 113. C. G. Hartinger, M. Groessl, S. M. Meier, A. Casini and P. J. Dyson, Application of mass spectrometric techniques to delineate the modes-of-action of anticancer metallodrugs, *Chem. Soc. Rev.*, 2013, **42**, 6186-6199.
 114. L. Messori and A. Merlino, Protein metalation by metal-based drugs: X-ray crystallography and mass spectrometry studies, *Chem. Commun.*, 2017, **53**, 11622-11633.
 115. A. Merlino, T. Marzo and L. Messori, Protein Metalation by Anticancer Metallodrugs: A Joint ESI MS and XRD Investigative Strategy, *Chem.-Eur. J.*, 2017, **23**, 6942-6947.
 116. F. Wang, J. Bella, J. A. Parkinson and P. J. Sadler, Competitive reactions of a ruthenium arene anticancer complex with histidine, cytochrome c and an oligonucleotide, *J. Biol. Inorg. Chem.*, 2005, **10**, 147-155.
 117. A. Casini, C. Gabbiani, G. Mastrobuoni, L. Messori, G. Moneti and G. Pieraccini, Exploring Metallodrug-Protein Interactions by ESI Mass Spectrometry: The Reaction of Anticancer Platinum Drugs with Horse Heart Cytochrome c, *ChemMedChem*, 2006, **1**, 413-417.
 118. A. Casini, C. Gabbiani, E. Michelucci, G. Pieraccini, G. Moneti, P. J. Dyson and L. Messori, Exploring metallodrug-protein interactions by mass spectrometry: comparisons between platinum coordination complexes and an organometallic ruthenium compound, *J. Biol. Inorg. Chem.*, 2009, **14**, 761-770.
 119. S. M. Meier, C. Gerner, B. K. Keppler, M. A. Cinellu and A. Casini, Mass Spectrometry Uncovers Molecular Reactivities of Coordination and Organometallic Gold(III) Drug Candidates in Competitive Experiments That Correlate with Their Biological Effects, *Inorg. Chem.*, 2016, **55**, 4248-4259.
 120. T. Pivetta, V. Lallai, E. Valletta, F. Trudu, F. Isaia, D. Perra, E. Pinna and A. Pani, Mixed copper-platinum complex formation could explain synergistic antiproliferative effect exhibited by binary mixtures of cisplatin and copper-1,10-phenanthroline compounds: An ESI-MS study, *J. Inorg. Biochem.*, 2015, **151**, 107-114.
 121. J. Contreras-García, E. R. Johnson, S. Keinan, R. Chaudret, J.-P. Piquemal, D. N. Beratan and W. Yang, NCIPLLOT: A Program for Plotting Noncovalent Interaction Regions, *J. Chem. Theory Comput.*, 2011, **7**, 625-632.
 122. T. Koleša-Dobravc, E. Lodyga-Chruscinska, M. Symonowicz, D. Sanna, A. Meden, F. Perdih and E. Garribba, Synthesis and Characterization of V^{IV}O Complexes of Picolinate and Pyrazine Derivatives. Behavior in the Solid State and Aqueous Solution and Biotransformation in the Presence of Blood Plasma Proteins, *Inorg. Chem.*, 2014, **53**, 7960-7976.
 123. E. Lodyga-Chruscinska, G. Micera and E. Garribba, Complex Formation in Aqueous Solution and in the Solid State of the Potent Insulin-Enhancing V^{IV}O²⁺ Compounds Formed by Picolinate and Quinolinate Derivatives, *Inorg. Chem.*, 2011, **50**, 883-899.
 124. C. Drennan, S. Huang, J. Drummond, R. Matthews and M. Lidwig, How a protein binds B12: A 3.0 Å X-ray structure of B12-binding domains of methionine synthase, *Science*, 1994, **266**, 1669-1674.
 125. D. Sanna, G. Micera and E. Garribba, Interaction of VO²⁺ Ion and Some Insulin-Enhancing Compounds with Immunoglobulin G, *Inorg. Chem.*, 2011, **50**, 3717-3728.
 126. D. Sanna, V. Ugone, G. Lubinu, G. Micera and E. Garribba, Behavior of the potential antitumor V^{IV}O complexes formed by flavonoid ligands. 1. Coordination modes and geometry in solution and at the physiological pH, *J. Inorg. Biochem.*, 2014, **140**, 173-184.
 127. H. Yasui, K. Takechi and H. Sakurai, Metallokinetic analysis of disposition of vanadyl complexes as insulin-mimetics in rats using BCM-ESR method, *J. Inorg. Biochem.*, 2000, **78**, 185-196.
 128. D. Sanna, J. Palomba, G. Lubinu, P. Buglyó, S. Nagy, F. Perdih and E. Garribba, Role of Ligands in the Uptake and Reduction of V(V) Complexes in Red Blood Cells, *J. Med. Chem.*, 2019, **62**, 654-664.
 129. D. C. Crans, J. J. Smees, E. Gaidamauskas and L. Yang, The Chemistry and Biochemistry of Vanadium and the Biological Activities Exerted by Vanadium Compounds, *Chem. Rev.*, 2004, **104**, 849-902.
 130. S. Al-Harhi, J. I. Lachowicz, M. E. Nowakowski, M. Jaremko and Ł. Jaremko, Towards the functional high-resolution coordination chemistry of blood plasma human serum albumin, *J. Inorg. Biochem.*, 2019, **198**, 110716.
 131. G. Sciortino, D. Sanna, G. Lubinu, J.-D. Maréchal and E. Garribba, Unveiling V^{IV}O²⁺ Binding Modes to Human Serum Albumins by an Integrated Spectroscopic-Computational Approach, *Chem.-Eur. J.*, 2020, **26**, 11316-11326.
 132. P. E. M. Siegbahn and F. Himo, The quantum chemical cluster approach for modeling enzyme reactions, *Wiley Interdiscip. Rev. Comput. Mol. Sci.*, 2011, **1**, 323-336.
 133. A. P. Ginsberg, Magnetic exchange in transition metal complexes. 12. Calculation of cluster exchange coupling constants with the X.alpha.-scattered wave method, *J. Am. Chem. Soc.*, 1980, **102**, 111-117.
 134. L. Noodleman, Valence bond description of antiferromagnetic coupling in transition metal dimers, *J. Chem. Phys.*, 1981, **74**, 5737-5743.
 135. J. R. Simard, P. A. Zunsain, J. A. Hamilton and S. Curry, Location of High and Low Affinity Fatty Acid Binding Sites on Human

- Serum Albumin Revealed by NMR Drug-competition Analysis, *J. Mol. Biol.*, 2006, **361**, 336-351.
136. A. A. Bhattacharya, T. Grüne and S. Curry, Crystallographic analysis reveals common modes of binding of medium and long-chain fatty acids to human serum albumin, *J. Mol. Biol.*, 2000, **303**, 721-732.
 137. S. Curry, P. Brick and N. P. Franks, Fatty acid binding to human serum albumin: new insights from crystallographic studies, *Biochim. Biophys. Acta, Mol. Cell Biol. Lipids*, 1999, **1441**, 131-140.
 138. J. P. C. Coverdale, J. P. Barnett, A. H. Adamu, E. J. Griffiths, A. J. Stewart and C. A. Blindauer, A metalloproteomic analysis of interactions between plasma proteins and zinc: elevated fatty acid levels affect zinc distribution, *Metallomics*, 2019, **11**, 1805-1819.
 139. C. A. Blindauer, I. Harvey, K. E. Bunyan, A. J. Stewart, D. Sleep, D. J. Harrison, S. Berezenko and P. J. Sadler, Structure, Properties, and Engineering of the Major Zinc Binding Site on Human Albumin, *J. Biol. Chem.*, 2009, **284**, 23116-23124.
 140. J. P. Barnett, C. A. Blindauer, O. Kassar, S. Khazaipoul, E. M. Martin, P. J. Sadler and A. J. Stewart, Allosteric modulation of zinc speciation by fatty acids, *Biochim. Biophys. Acta, Gen. Subj.*, 2013, **1830**, 5456-5464.
 141. D. Sanna, E. Garribba and G. Micera, Interaction of VO²⁺ ion with human serum transferrin and albumin, *J. Inorg. Biochem.*, 2009, **103**, 648-655.
 142. I. Correia, T. Jakusch, E. Cobbinna, S. Mehtab, I. Tomaz, N. V. Nagy, A. Rockenbauer, J. Costa Pessoa and T. Kiss, Evaluation of the binding of oxovanadium(IV) to human serum albumin, *Dalton Trans.*, 2012, **41**, 6477-6487.
 143. G. C. Justino, E. Garribba and J. Costa Pessoa, Binding of V^{IVO}2+ to the Fe binding sites of human serum transferrin. A theoretical study, *J. Biol. Inorg. Chem.*, 2013, **18**, 803-813.
 144. V. Ugone, D. Sanna, G. Sciortino, J.-D. Maréchal and E. Garribba, Interaction of Vanadium(IV) Species with Ubiquitin: A Combined Instrumental and Computational Approach, *Inorg. Chem.*, 2019, **58**, 8064-8078.
 145. G. Sciortino, D. Sanna, V. Ugone, J.-D. Maréchal and E. Garribba, Integrated ESI-MS/EPR/computational characterization of the binding of metal species to proteins: vanadium drug-myoglobin application, *Inorg. Chem. Front.*, 2019, **6**, 1561-1578.
 146. D. Rehder, Perspectives for vanadium in health issues, *Future Med. Chem.*, 2016, **8**, 325-338.
 147. R. K. Narla, Y. Dong, D. Klis and F. M. Uckun, *In vivo* antitumor activity of bis(4,7-dimethyl-1,10-phenanthroline) sulfatooxovanadium(IV) {METVAN [VO(SO₄)(Me₂Phen)₂]}, *Clin. Cancer Res.*, 2001, **7**, 2124-2133.
 148. D. A. Barrio and S. B. Etcheverry, Potential Use of Vanadium Compounds in Therapeutics, *Curr. Med. Chem.*, 2010, **17**, 3632-3642.
 149. D. Sanna, V. Ugone, G. Micera, P. Buglyó, L. Bíró and E. Garribba, Speciation in human blood of Metvan, a vanadium based potential anti-tumor drug, *Dalton Trans.*, 2017, **46**, 8950-8967.
 150. G. Sciortino, D. Sanna, V. Ugone, J.-D. Maréchal, M. Alemany-Chavarria and E. Garribba, Effect of secondary interactions, steric hindrance and electric charge on the interaction of V^{IVO} species with proteins, *New J. Chem.*, 2019, **43**, 17647-17660.
 151. M. Rangel, A. Tamura, C. Fukushima and H. Sakurai, *In vitro* study of the insulin-like action of vanadyl-pyrone and -pyridinone complexes with a VO(O₄) coordination mode, *J. Biol. Inorg. Chem.*, 2001, **6**, 128-132.
 152. C. Rozzo, D. Sanna, E. Garribba, M. Serra, A. Cantara, G. Palmieri and M. Pisano, Antitumoral effect of vanadium compounds in malignant melanoma cell lines, *J. Inorg. Biochem.*, 2017, **174**, 14-24.
 153. P. Buglyó, T. Kiss, E. Kiss, D. Sanna, E. Garribba and G. Micera, Interaction between the low molecular mass components of blood serum and the VO(IV)-DHP system (DHP = 1,2-dimethyl-3-hydroxy-4(1H)-pyridinone), *J. Chem. Soc., Dalton Trans.*, 2002, 2275-2282.
 154. M. Rangel, A. Leite, M. J. Amorim, E. Garribba, G. Micera and E. Lodyga-Chruscinska, Spectroscopic and potentiometric characterization of oxovanadium(IV) complexes formed by 3-hydroxy-4-pyridinones. Rationalization of the influence of basicity and electronic structure of the ligand on the properties of V^{IVO} species in aqueous solution, *Inorg. Chem.*, 2006, **45**, 8086-8097.
 155. H. M. Berman, J. Westbrook, Z. Feng, G. Gilliland, T. N. Bhat, H. Weissig, I. N. Shindyalov and P. E. Bourne, The Protein Data Bank, *Nucleic Acids Res.*, 2000, **28**, 235-242.
 156. B. Bueloni, D. Sanna, E. Garribba, G. R. Castro, I. E. León and G. A. Islan, Design of nalidixic acid-vanadium complex loaded into chitosan hybrid nanoparticles as smart strategy to inhibit bacterial growth and quorum sensing, *Int. J. Biol. Macromol.*, 2020, **161**, 1568-1580.
 157. D. Sanna, V. Ugone, G. Sciortino, P. Buglyó, Z. Bihari, P. L. Parajdi-Losonczí and E. Garribba, V^{IVO} complexes with antibacterial quinolone ligands and their interaction with serum proteins, *Dalton Trans.*, 2018, **47**, 2164-2182.
 158. V. Ugone, D. Sanna, S. Ruggiu, G. Sciortino and E. Garribba, Covalent and non-covalent binding in vanadium-proteins adducts, *Inorg. Chem. Front.*, DOI: 10.1039/D1030QJ01308K.
 159. E. N. Kitova, A. El-Hawiet, P. D. Schnier and J. S. Klassen, Reliable Determinations of Protein-Ligand Interactions by Direct ESI-MS Measurements. Are We There Yet?, *J. Am. Soc. Mass Spectrom.*, 2012, **23**, 431-441.
 160. K. Elvingson, A. González Baró and L. Pettersson, Speciation in Vanadium Bioinorganic Systems. 2. An NMR, ESR, and Potentiometric Study of the Aqueous H⁺-Vanadate-Maltol System, *Inorg. Chem.*, 1996, **35**, 3388-3393.
 161. E. Irving and A. W. Stoker, Vanadium Compounds as PTP Inhibitors, *Molecules*, 2017, **22**, 2269.
 162. E. De Boer, K. Boon and R. Wever, Electron paramagnetic resonance studies on conformational states and metal ion exchange properties of vanadium bromoperoxidase, *Biochemistry*, 1988, **27**, 1629-1635.
 163. E. De Boer, C. P. Keijzers, A. A. K. Klaassen, E. J. Reijerse, D. Collison, C. D. Garner and R. Wever, ¹⁴N-coordination to VO²⁺ in reduced vanadium bromoperoxidase, an electron spin echo study, *FEBS Lett.*, 1988, **235**, 93-97.
 164. G. Sciortino and E. Garribba, The binding modes of V^{IVO}2+ ions in blood proteins and enzymes, *Chem. Commun.*, 2020, **56**, 12218-12221.
 165. C. Bisson, K. L. Britton, S. E. Sedelnikova, H. F. Rodgers, T. C. Eadsforth, R. C. Viner, T. R. Hawkes, P. J. Baker and D. W. Rice, Crystal Structures Reveal that the Reaction Mechanism of Imidazoleglycerol-Phosphate Dehydratase Is Controlled by Switching Mn(II) Coordination, *Structure*, 2015, **23**, 1236-1245.
 166. J. Petersen, T. R. Hawkes and D. J. Lowe, Oxo-vanadium as a spin probe for the investigation of the metal coordination

- environment of imidazole glycerol phosphate dehydratase, *J. Inorg. Biochem.*, 2000, **80**, 161-168.
167. F. van de Velde and L. Könemann, Enantioselective sulfoxidation mediated by vanadium-incorporated phytase: a hydrolase acting as a peroxidase, *Chem. Commun.*, 1998, 1891-1892.
 168. G. Zampella, P. Fantucci, V. L. Pecoraro and L. De Gioia, Insight into the Catalytic Mechanism of Vanadium Haloperoxidases. DFT Investigation of Vanadium Cofactor Reactivity, *Inorg. Chem.*, 2006, **45**, 7133-7143.
 169. Y. Zhang and J. A. Gascón, QM/MM investigation of structure and spectroscopic properties of a vanadium-containing peroxidase, *J. Inorg. Biochem.*, 2008, **102**, 1684-1690.
 170. G. A. Anderson, R. N. Behera and R. Gomatam, Calculation of higher protonation states and of a new resting state for vanadium chloroperoxidase using QM/MM, with an Atom-in-Molecules analysis, *J. Mol. Graph. Model.*, 2020, **99**, 107624.
 171. W. Hemrika, R. Renirie, S. Macedo-Ribeiro, A. Messerschmidt and R. Wever, Heterologous Expression of the Vanadium-containing Chloroperoxidase from *Curvularia inaequalis* in *Saccharomyces cerevisiae* and Site-directed Mutagenesis of the Active Site Residues His496, Lys353, Arg360, and Arg490, *J. Biol. Chem.*, 1999, **274**, 23820-23827.
 172. G. Zampella, P. Fantucci, V. L. Pecoraro and L. De Gioia, Reactivity of Peroxo Forms of the Vanadium Haloperoxidase Cofactor. A DFT Investigation, *J. Am. Chem. Soc.*, 2005, **127**, 953-960.
 173. L. F. Pacios and O. Gálvez, Active Site, Catalytic Cycle, and Iodination Reactions of Vanadium Iodoperoxidase: A Computational Study, *J. Chem. Theory Comput.*, 2010, **6**, 1738-1752.
 174. G. Sciortino, J.-E. Sanchez-Aparicio, J. Rodríguez-Guerra Pedregal, E. Garribba and J.-D. Maréchal, Computational insight on the interaction of oxaliplatin with insulin, *Metallomics*, 2019, **11**, 765-773.
 175. M. B. Đukić, M. S. Jeremić, I. P. Filipović, O. R. Klisurić, V. V. Kojić, D. S. Jakimov, R. M. Jelić, V. Onnis and Z. D. Matović, Synthesis, characterization, HSA/DNA interactions and antitumor activity of new $[\text{Ru}(\eta^6\text{-}p\text{-cymene})\text{Cl}_2(\text{L})]$ complexes, *J. Inorg. Biochem.*, 2020, **213**, 111256.
 176. T. Di Meo, K. Kariyawasam, W. Ghattas, M. Valerio-Lepiniec, G. Sciortino, J.-D. Maréchal, P. Minard, J.-P. Mahy, A. Urvoas and R. Ricoux, Functionalized Artificial Bidomain Proteins Based on an α -Solenoid Protein Repeat Scaffold: A New Class of Artificial Diels-Alderases, *ACS Omega*, 2019, **4**, 4437-4447.
 177. G. Faa, C. Gerosa, D. Fanni, J. I. Lachowicz and V. M. Nurchi, Gold - Old Drug with New Potentials, *Curr. Med. Chem.*, 2018, **25**, 75-84.
 178. M. Porchia, M. Pellei, M. Marinelli, F. Tisato, F. Del Bello and C. Santini, New insights in Au-NHCs complexes as anticancer agents, *Eur. J. Med. Chem.*, 2018, **146**, 709-746.
 179. C. Yeo, K. Ooi and E. Tiekink, Gold-Based Medicine: A Paradigm Shift in Anti-Cancer Therapy?, *Molecules*, 2018, **23**, 1410.
 180. J. Christodoulou, P. J. Sadler and A. Tucker, ^1H NMR of albumin in human blood plasma: drug binding and redox reactions at Cys34, *FEBS Lett.*, 1995, **376**, 1-5.
 181. J. R. Roberts, J. Xiao, B. Schliesman, D. J. Parsons and C. F. Shaw, Kinetics and Mechanism of the Reaction between Serum Albumin and Auranofin (and Its Isopropyl Analogue) in Vitro, *Inorg. Chem.*, 1996, **35**, 424-433.
 182. T. C. Dean, M. Yang, M. Liu, J. M. Grayson, A. W. DeMartino, C. S. Day, J. Lee, C. M. Furdul and U. Bierbach, Human Serum Albumin-Delivered $[\text{Au}(\text{PET}_3)]^+$ Is a Potent Inhibitor of T Cell Proliferation, *ACS Med. Chem. Lett.*, 2017, **8**, 572-576.
 183. A. Pratesi, D. Cirri, D. Fregona, G. Ferraro, A. Giorgio, A. Merlino and L. Messori, Structural Characterization of a Gold/Serum Albumin Complex, *Inorg. Chem.*, 2019, **58**, 10616-10619.
 184. I. Tolbatov, D. Cirri, L. Marchetti, A. Marrone, C. Coletti, N. Re, D. La Mendola, L. Messori, T. Marzo, C. Gabbiani and A. Pratesi, Mechanistic Insights Into the Anticancer Properties of the Auranofin Analog $\text{Au}(\text{PET}_3)$: A Theoretical and Experimental Study, *Front. Chem.*, 2020, **8**.
 185. C. Zoppi, L. Messori and A. Pratesi, ESI MS studies highlight the selective interaction of Auranofin with protein free thiols, *Dalton Trans.*, 2020, **49**, 5906-5913.
 186. J. Zou, P. Taylor, J. Dornan, S. P. Robinson, M. D. Walkinshaw and P. J. Sadler, First Crystal Structure of a Medicinally Relevant Gold Protein Complex: Unexpected Binding of $[\text{Au}(\text{PET}_3)]^+$ to Histidine, *Angew. Chem., Int. Ed.*, 2000, **39**, 2931-2934.
 187. L. Chiniadis, I. Bratsos, K. Bethanis, M. Karpusas, P. Giastas and A. Papakyriakou, High-resolution crystal structures of a "half sandwich"-type $\text{Ru}(\text{II})$ coordination compound bound to hen egg-white lysozyme and proteinase K, *J. Biol. Inorg. Chem.*, 2020, **25**, 635-645.
 188. A. Guellouz, M. Valerio-Lepiniec, A. Urvoas, A. Chevrel, M. Graille, Z. Fourati-Kammoun, M. Desmadril, H. van Tilbeurgh and P. Minard, Selection of Specific Protein Binders for Pre-Defined Targets from an Optimized Library of Artificial Helicoidal Repeat Proteins (αRep), *PLoS One*, 2013, **8**, e71512.
 189. A. Urvoas, A. Guellouz, M. Valerio-Lepiniec, M. Graille, D. Durand, D. C. Desravines, H. van Tilbeurgh, M. Desmadril and P. Minard, Design, Production and Molecular Structure of a New Family of Artificial α -helicoidal Repeat Proteins (αRep) Based on Thermostable HEAT-like Repeats, *J. Mol. Biol.*, 2010, **404**, 307-327.
 190. A. Einstein, *Ideas and Opinions, 5th Ed.*, Crown Publishers, Inc., New York, 1960.